

University of Kentucky

UKnowledge

Theses and Dissertations--Mining Engineering

Mining Engineering


2022

PARAMETRIC NUMERICAL ANALYSIS OF INCLINED COAL PILLARS

Robin Flattery

robin.flattery94@gmail.com

Author ORCID Identifier:

 <https://orcid.org/0000-0001-8547-5053>

Digital Object Identifier: <https://doi.org/10.13023/etd.2022.461>

[Right click to open a feedback form in a new tab to let us know how this document benefits you.](#)

Recommended Citation

Flattery, Robin, "PARAMETRIC NUMERICAL ANALYSIS OF INCLINED COAL PILLARS" (2022). *Theses and Dissertations--Mining Engineering*. 73.

https://uknowledge.uky.edu/mng_etds/73

This Master's Thesis is brought to you for free and open access by the Mining Engineering at UKnowledge. It has been accepted for inclusion in Theses and Dissertations--Mining Engineering by an authorized administrator of UKnowledge. For more information, please contact UKnowledge@lsv.uky.edu.

STUDENT AGREEMENT:

I represent that my thesis or dissertation and abstract are my original work. Proper attribution has been given to all outside sources. I understand that I am solely responsible for obtaining any needed copyright permissions. I have obtained needed written permission statement(s) from the owner(s) of each third-party copyrighted matter to be included in my work, allowing electronic distribution (if such use is not permitted by the fair use doctrine) which will be submitted to UKnowledge as Additional File.

I hereby grant to The University of Kentucky and its agents the irrevocable, non-exclusive, and royalty-free license to archive and make accessible my work in whole or in part in all forms of media, now or hereafter known. I agree that the document mentioned above may be made available immediately for worldwide access unless an embargo applies.

I retain all other ownership rights to the copyright of my work. I also retain the right to use in future works (such as articles or books) all or part of my work. I understand that I am free to register the copyright to my work.

REVIEW, APPROVAL AND ACCEPTANCE

The document mentioned above has been reviewed and accepted by the student's advisor, on behalf of the advisory committee, and by the Director of Graduate Studies (DGS), on behalf of the program; we verify that this is the final, approved version of the student's thesis including all changes required by the advisory committee. The undersigned agree to abide by the statements above.

Robin Flattery, Student

Dr. Zach Agioutantis, Major Professor

Dr. Jhon Silva, Director of Graduate Studies

PARAMETRIC NUMERICAL ANALYSIS OF INCLINED COAL PILLARS

THESIS

A thesis submitted in partial fulfillment of the
requirements for the degree of Master of Science in the
Mining Engineering in the College of Engineering
at the University of Kentucky

By

Robin Julian Flattery

Lexington, Kentucky

Director: Dr. Zach Agioutantis, Professor of Mining Engineering

Lexington, Kentucky

2022

Copyright © Robin Julian Flattery 2022
[<https://orcid.org/0000-0001-8547-5053>]

ABSTRACT OF THESIS

PARAMETRIC NUMERICAL ANALYSIS OF INCLINED COAL PILLARS

Pillars are used as the primary support structures for underground mining to maintain stability by supporting the overlying strata. In the case of horizontal seams, the pillars are typically subjected to axial loading due to the weight of the overburden and/or abutment stresses, while in the case of inclined seams they are subjected to oblique loading due to both the vertical and horizontal in-situ stress. Over the years numerous studies have been completed on square and rectangular pillars in horizontal seams that have resulted in several pillar stability equations and criteria. However very few studies are available with respect to pillars in inclined seams. Inclined pillars are subject not only to high normal stresses, but they are also subject to higher shear stresses that depend on the inclination of the seam, the ratio of the horizontal to vertical in-situ stress as well as the physical and mechanical properties of the material. This work presents a parametric numerical investigation of pillars in inclined seams using the finite element method (FEM) by evaluating different geometrical parameters such as seam inclination, pillar rib geometry as well as different pillar strength parameters. The major principal stress was examined at mid height of the center pillar whereas the rotational shear stress was taken at the roof-pillar interface of the center pillar. It is concluded that under Hoek & Brown conditions, high shear stress is developed at the pillar-roof interface for inclined pillars and such stress increase as pillar inclination increases. The shear stress developed in the pillar roof interface for the Hoek & Brown models does not peak at the uphill pillar rib, compared to the elastic models. The shear stress is slightly higher on the uphill side of inclined pillars than on the downhill side. Finally, the major principal stress at the ribs is higher for the elastic models than the Hoek & Brown models.

Keywords: Inclined pillars, Numerical modelling, Shear stresses, Major principal stresses.

Robin Julian Flattery

12/15/2022

Date

PARAMETRIC NUMERICAL ANALYSIS OF INCLINED COAL PILLARS

By
Robin Julian Flattery

Dr. Zach Agioutantis

Director of Thesis

Dr. Jhon Silva Castro

Director of Graduate Studies

12/15/2022

Date

DEDICATION

To my parents Julian and Ezna, and my sister Angelique for always encouraging me to challenge myself and reach my full potential. Likewise, this thesis is dedicated to Elze, for all her love and support.

ACKNOWLEDGMENTS

Appreciation and sincere thanks are hereby expressed to:

- The Creator, for good health, insight, and guidance.
- My advisor, Dr Zach Agioutantis, for his able guidance, patience, and encouragement.
- My committee members, Dr. Steven Schafrik and Dr. Jhon Silva.
- Dr Andre Vervoort, from the University of Leuven, for pointing out key points in this study.
- My parents, for their sacrifice, patience, and interest.
- To friends and colleagues who have not been mentioned by name but was helpful with the final preparation, printing, advice, and counsel.

Thank you very much!

CONTRIBUTIONS TO THE LITERATURE

Below is a listing of the papers that were contributed to the literature based on the research presented in this thesis:

1. Flattery R. and Z. Agioutantis, Inclined Pillar Strength Considerations: Review of Different Methodologies, SME Preprint No 22-037, SME Annual Meeting, February 27-March 2, 2022, Salt Lake City, UT.
2. Flattery, R., Z. Agioutantis, and K. Kaklis, Parametric numerical analysis on inclined pillars, Proceedings, 41st International Conference on Ground Control in Mining, July 26-28, 2022, Canonsburg, PA.

TABLE OF CONTENTS

ACKNOWLEDGMENTS	v
CONTRIBUTIONS TO THE LITERATURE	vi
LIST OF TABLES	ix
LIST OF FIGURES	x
CHAPTER 1. INTRODUCTION	1
CHAPTER 2. BACKGROUND AND LITERATURE REVIEW	2
2.1 <i>In-situ stress</i>	3
2.2 <i>Pillar stresses</i>	4
2.2.1 Numerical modeling	5
2.2.1.1 Numerical modeling overview	5
2.2.1.2 Numerical modeling application	6
2.2.2 Analytical methods	9
2.2.2.1 Tributary area method for horizontal seams	9
2.2.2.2 Tributary area method for inclined seams	12
2.2.2.3 Limitations of using the tributary method	15
2.2.3 Other methods	15
2.3 <i>Intact rock strength</i>	16
2.3.1 Mohr-Coulomb failure criterion	16
2.3.2 Hoek & Brown failure criterion	17
2.3.3 Mohr-Coulomb vs Hoek & Brown failure criteria	17
2.4 <i>Pillar strength</i>	19
2.4.1 Horizontal pillars	19
2.4.2 Inclined pillars	26
2.4.2.1 Analytical solutions	26
2.4.2.2 Laboratory testing	27
2.4.2.3 Numerical solutions	29
2.5 <i>Stability factor</i>	30
CHAPTER 3. NUMERICAL MODELING	33
3.1 <i>Model development</i>	33
3.2 <i>Numerical Analysis</i>	37

CHAPTER 4. RESULTS AND DISCUSSION.....	41
4.1 <i>Major principal stress</i>	41
4.1.1 Major principal stress under elastic conditions.....	41
4.1.2 Major principal stress under the Hoek & Brown criterion	46
4.1.3 Comparison between the elastic and Hoek & Brown models.....	51
4.2 <i>Shear stress at the pillar-roof interface</i>	53
4.2.1 Rotated shear stress at the pillar-roof interface under elastic conditions.....	54
4.2.2 Rotated shear stress at the pillar roof interface using the Hoek & Brown criterion	56
4.2.3 Comparison between the elastic and Hoek & Brown models.....	59
4.3 <i>Summary of numerical results</i>	59
CHAPTER 5. CONCLUSIONS AND RECOMMENDATIONS.....	67
5.1 <i>Conclusions</i>	67
5.2 <i>Recommendations</i>	68
REFERENCES	69
VITA.....	74

LIST OF TABLES

Table 2.1: Different in-situ field-testing techniques (Aadnøy & Looyeh 2019).	4
Table 2.2: Several pillar strength equations.....	20
Table 3.1: Elastic parameters of sandstone (Tulu et al., 2017).....	35
Table 3.2: Elastic parameters of coal (Esterhuizen et al., 2010).....	35
Table 3.3: Material properties for Hoek-Brown Constitutive Model (Esterhuizen et al.,2010).	36
Table 3.4: Material properties for the interface element (Esterhuizen et al., 2010).	37
Table 4.1: Summary of the major principal stress results under elastic conditions.....	60
Table 4.2: Summary of the major principal stress results under Hoek & Brown conditions.....	61
Table 4.3: Summary of the shear stress results under elastic conditions.....	63
Table 4.4: Summary of the shear stress results under Hoek & Brown conditions.	64

LIST OF FIGURES

Figure 2.1: In-situ stress in a rock formation (Aadnøy & Looyeh, 2019).	3
Figure 2.2: Horizontal pillars subjected to compression loading (Jessu & Spearing, 2019).	4
Figure 2.3: Inclined pillars subjected to oblique loading (Jessu & Spearing, 2019).	5
Figure 2.4: Brittle and shear failure modes in pillars (Esterhuizen, 2006).	7
Figure 2.5: Pillars subjected to normal loading and oblique loading (Hedley et al., 1984).	8
Figure 2.6: Stress distribution in the pillar when the far-field principal stresses are oriented at an angle to the pillar (Suorinen et al., 2011).	8
Figure 2.7: Tributary method explained for a room and pillar mining layout (Foroughi, 1996).	11
Figure 2.8: Inclined seam with pillar ribs perpendicular to the roof (Foroughi, 1996). ...	12
Figure 2.9: Inclined seam with deviating pillar rib angles (Foroughi, 1996).	14
Figure 2.10: (a) shows a Hoek & Brown elastic-brittle-plastic rockmass behavior and (b) a Mohr-Coulomb elastic-perfectly-plastic rockmass behavior (Saiang et al., 2014).	18
Figure 2.11: The strength change of the (a) gypsum samples, (b) sandstone samples for various width to height ratios and various inclinations (Jessu et al., 2018).	27
Figure 2.12: Strength reduction for gypsum and sandstone (derived from Jessu et al., 2018)	28
Figure 2.13: Shows (a) the cushion blocks used in the experimental setup, and (b) the UCS results (Luo et al., 2020).	28
Figure 2.14: The relationship between pillar strength, pillar stress and stability factor (Suorinen, 2013).	31
Figure 2.15: Effect of gradient on pillar stability (Merwe et al. 2002).	31
Figure 3.1: Geometry of models developed.	34
Figure 3.2: Model of a 20° inclined pillar with vertical pillar ribs (A-Pillar).	34
Figure 3.3: Model of a 20° inclined pillar with pillar ribs perpendicular to the floor (B- Pillar).	35
Figure 3.4: Shows the interface elements that was added between the sandstone and the coal.	37
Figure 3.5: Model of the Horizontal pillar dimensions.	38
Figure 3.6: Model of five 20° Inclined A-pillars.	38
Figure 3.7: Left: Mesh with a gradation factor of 0.1. Right: Mesh with a gradation factor of 0.01.	39
Figure 3.8: Increased mesh discretization density around the center pillar.	39
Figure 3.9: Model geometries for elastic models.	40
Figure 3.10: Model geometries for Hoek & Brown models.	40
Figure 4.1: Location of the major principal stress queries.	41
Figure 4.2: Elastic major principal stress results.	42
Figure 4.3: Elastic major principal stress results for a 30° inclined A- and B-Pillar.	43

Figure 4.4: Orientation of the major principal stress for an elastic flat pillar.....	43
Figure 4.5: Orientation of the major principal stress for an elastic 30° inclined A-Pillar.....	44
Figure 4.6: Displacement vectors for an elastic flat pillar.	45
Figure 4.7: Displacement vectors for an elastic 30° inclined A-Pillar.	45
Figure 4.8: Variation of the major principal stress along the pillar width at mid height for the Hoek & Brown models for different coal UCS values for the horizontal pillar.	46
Figure 4.9: Variation of the major principal stress along the pillar width at mid height for the Hoek & Brown models for different coal UCS values for the 20° inclined A- Pillar.	47
Figure 4.10: Comparison of the major principal stress and different inclination with a vertical pillar geometry (A-Pillar), with a coal UCS of 20 MPa.	48
Figure 4.11: Variation of the major principal stress along the pillar width at mid height for the Hoek & Brown models in the case of the 20° inclined A- and B-Pillar, with a coal UCS of 20 MPa.	48
Figure 4.12: Orientation of the major principal stress for a 15 MPa Hoek & Brown flat pillar.	49
Figure 4.13: Orientation of the major principal stress for a 15 MPa Hoek & Brown 20° A-Pillar.....	49
Figure 4.14: Displacement vectors for a 15 MPa Hoek & Brown flat pillar.	50
Figure 4.15: Displacement vectors for a 15 MPa Hoek & Brown 20° A-Pillar.	51
Figure 4.16: Comparison of the major principal stress between the elastic and Hoek & Brown models for a flat pillar and 20° inclined A-Pillar.....	52
Figure 4.17: Location of the shear stress queries.....	53
Figure 4.18: Stress element.....	54
Figure 4.19: Variation of the shear stress along the pillar-roof interface with respect to the seam inclination in elastic models.	55
Figure 4.20: Variation of the shear stress along the pillar-roof interface for elastic models in the case of the 30° inclined A- and B-Pillar.	56
Figure 4.21: Variation of the shear stress along the pillar-roof interface with respect to the pillar inclination for Hoek & Brown models with coal UCS = 20 MPa.....	57
Figure 4.22: Variation of the shear stress along the pillar-roof interface with respect to the pillar inclination for Hoek & Brown models with coal UCS = 10 MPa.....	58
Figure 4.23: Variation of the shear stress along the pillar-roof interface with respect a 30° pillar inclination Hoek & Brown models with coal UCS = 20 MPa for A-Pillar and B-Pillar.....	58
Figure 4.24: Comparison of the shear stress between the elastic and Hoek & Brown models for a flat pillar and 20° inclined A-Pillar.....	59
Figure 4.25: Major principal stress under elastic conditions.	60
Figure 4.26: Peak major principal stress results under Hoek & Brown conditions.....	62
Figure 4.27: Mid pillar major principal stress results under Hoek & Brown conditions..	63
Figure 4.28: The peak and mid pillar shear stress results under elastic conditions.....	64
Figure 4.29: Peak shear stress results under Hoek & Brown conditions.	66
Figure 4.30: Mid pillar shear stress result under Hoek & Brown conditions.	66

CHAPTER 1. INTRODUCTION

Coal or rock pillars have various functions in mining operations; they act as the primary support structure, help to keep airways open for ventilation purposes, and reduce or eliminate surface subsidence (Luo et al., 2020). It is almost impossible to mine safely without appropriately designed pillars. Poor design of mine pillars may result in roof falls, floor heaves, pillar bursts, rib rolls, surface subsidence, and other events which may put miners and equipment at risk.

Due to the complex loading environment in a mine, mine pillars are subjected to different stresses. A horizontal pillar will typically experience normal (vertical) stresses whereas an inclined pillar will experience a combination of normal and shear stresses. The stresses on a pillar might also change with time. Mining is an active and ongoing process, where the faces are always advancing. This means that the stresses acting on a pillar will always change. A pillar that is designed and constructed for given loading conditions may not always be subjected to the same stresses during the life of the mine. It is possible that a pillar may also be subjected to shear stresses, either of static or dynamic nature (Maritz, 2015).

Pillar strength can be estimated through several empirical formulas that are available in the literature. These formulas are typically based on a statistical analysis of case study data. The limitations of most of these equations are that they only considered the width to height ratio and in-situ rock or coal strength for square or rectangular pillars in horizontal seams. The implementation of such equations to estimate pillar strength in inclined seams may overestimate the pillar strength and ultimately lead to an unstable pillar.

This thesis presents a parametric numerical analysis of pillars in inclined seams using the finite element method by evaluating different geometrical parameters, i.e., seam inclination, and different pillar strength parameters.

Chapter details

This thesis consists out of five chapters. The heading of each chapter is listed below:

- Chapter 1 presents the introduction.
- Chapter 2 present the background and the literature review.
- Chapter 3 presents the model development.
- Chapter 4 presents the results and the discussion.
- Chapter 5 presents the conclusions and recommendations.

CHAPTER 2. BACKGROUND AND LITERATURE REVIEW

An underground mine pillar can be described as "the in-situ rock between two or more underground openings" (Coates, 1981). Depending on the mining method and the mine orebody, mine pillars have different functions (Maybee, 2000). Barrier pillars are used to give regional support dividing orebodies into panels. Rib pillars are used to separate, and to provide support to openings. In cut and fill operations post pillars are used for local support. In steeply dipping orebodies, sill pillars are used to separate the orebody in various mining levels and the crown pillars prevent the rockmass above the mine from collapsing.

Even though mine pillars have an essential role in the mining industry, their design still have significant challenges. Pillar design is dependent on pillar strength and the pillar stress (Esterhuizen et al., 2008). For stable pillars the pillar strength should always be higher than the stress exerted on the pillar. The stability factor relates the average pillar strength to the average pillar stress for a flat orebody. Some of the factors that influence pillar stability are the depth of the orebody, the excavation size, horizontal stresses, rockmass properties, orebody, inclination, and backfilling (Kaklis et al., 2021). It is additionally understood that with an active advancing face, a continuous re-distribution of stresses occurs to maintain equilibrium. It is anticipated that a pillar, which is designed and intended to only experience normal loading environments, will not always be in this "ideal" setting, and during some stages of mining, shear stresses would also form part of the loading system. The magnitude of pillar stress will depend on different conditions such as jointing within the pillar, roof, and floor conditions, the dip of the orebody, loading system, vertical and the horizontal stresses, length to width ratio, and pillar dimensions (Maritz, 2015).

Numerous research on pillar size, shape, and stability under normal loading conditions have been conducted. For room-and-pillar granite mines, Hedley and Grant (1972) formulated an empirical relationship that correlates pillar strength and width-to-height ratio. Lunder & Pakalnis, (1997) have considered the role of confinement in determining the strength of hard rock pillars. Maybee, (2000) conducted numerous numerical studies and concluded that the pillar strength decreases with seam inclination. Esterhuizen et al., (2008) found that for limestone room-and-pillar mines, slender pillars have varying strengths depending on the geological composition, while there is little effect on squat pillars.

Jessu and Spearing (2018) indicated that limited research has been done on inclined rectangular pillars. Several mining companies are adopting these equations on inclined orebodies. A study done by Maritz (2015), indicated that various South African platinum mines adopted the Hedley and Grant (1972) equation for hard rock mining, which resulted in pillar failures. The conclusion of the study contradicts the argument that only normal stresses need to be considered in the factor of safety calculations. A study done by Lorig and Cabrera (2013) indicates that empirical pillar strength curves cannot be used for inclined/foliated pillars since pillar design curves do not account for inclined orebodies, square pillars, or weak hanging and footwalls. Failure to account for the effect of shear stress on pillar capacity may result in under-designed pillars, leading to pillar failure (Garza-Cruz et al., 2019).

2.1 In-situ stress

Rocks experience various stresses at any depth below the ground surface. Depending on the source that the stresses originated from as well as the depth below surface the stresses can vary in magnitude. In undisturbed ground, before any drilling or mining has taken place, the rock formation will usually be exposed to compressive stresses. This condition is recognized as in-situ stresses. Any point underground is generally subjected to three mutually perpendicular stresses. The vertical stress (σ_v) is primarily due to the depth below surface and the weight of the overburden. The vertical stress typically results in horizontal stresses due to the Poisson effect. When rock anisotropy as well as in-situ tectonic conditions are taken into account, two different horizontal (lateral) stresses may develop. These are typically depicted as σ_H and σ_h , normally referred to as maximum and minimum horizontal stresses (Aadnøy & Looyeh, 2019).

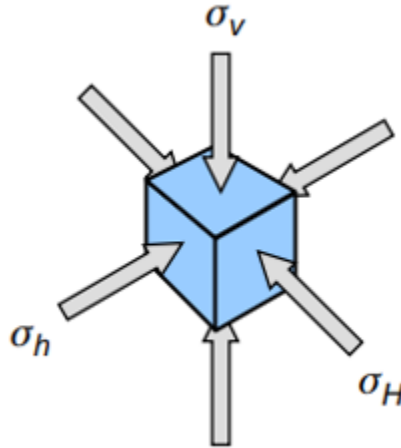


Figure 2.1: In-situ stress in a rock formation (Aadnøy & Looyeh, 2019).

There are several field test methods that are used to measure the orientation and the direction of in-situ stresses. These methods typically require a minimum of six measurements along different axes and independent of each other in order to calculate the resulting stress state tensor. According to Aadnøy & Looyeh (2019) there are mainly two approaches used to determine in-situ stresses, direct and indirect. Table 2.1 lists the different in-situ field testing techniques.

Table 2.1: Different in-situ field-testing techniques (Aadnøy & Looyeh 2019).

Direct testing	Indirect testing
Hydraulic fracturing	Acoustic emissions
Flat jack test	Borehole breakouts
Overcoring gauge test that was introduced by the United States Bureau of Mines (USBM)	Fault plane solutions
Overcoring gauge test introduced by the Commonwealth Scientific and Industrial Research Organization (CSIRO) in Australia	Differential strain analysis
	Inelastic strain relaxation
	Core diskings
	Observation of discontinuities

2.2 Pillar stresses

When an opening is made in the rockmass the in-situ (virgin or far-field) stresses are disturbed, causing the stresses to redistribute in the vicinity of the excavation. This is known as induced stresses (Foroughi, 1996). The stresses in rockmass are an important consideration when designing of underground pillars. The pillar stress depends on the depth and the extraction ratio of the mining activity. The tributary area theory is a popular approach for determining pillar stresses, and it is applied to situations where similar-sized pillars are developed in a large regular array in flat lying orebodies (Mgumbwa et al., 2010). Pillars in horizontal seams are mostly subjected to compressive stresses as shown in Figure 2.2.

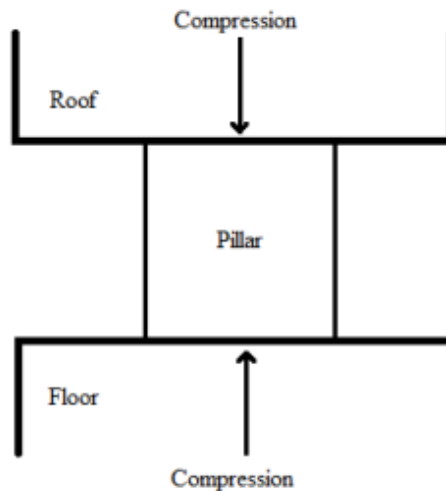


Figure 2.2: Horizontal pillars subjected to compression loading (Jessu & Spearing, 2019).

Mine pillars on inclined seams will experience oblique loading which is a combination of combined compression and shear loading. This is shown in Figure 2.3. It is very important to estimate the stresses that act on the inclined pillars since it will influence the pillars stability factor that is discussed in Section 2.5. However, due to the inclination it makes it difficult to estimate the stresses inside inclined pillars.

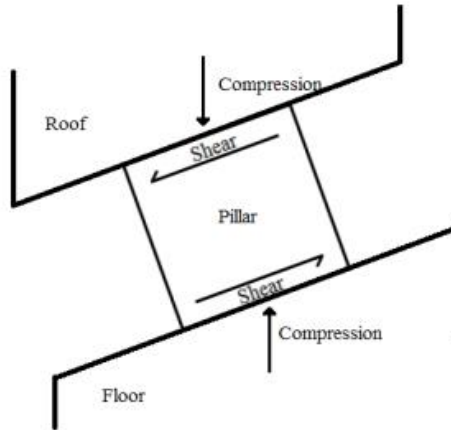


Figure 2.3: Inclined pillars subjected to oblique loading (Jessu & Spearing, 2019).

Throughout the literature there are different methods of estimating stresses in horizontal and inclined pillars. These methods include numerical modeling and analytical methods.

2.2.1 Numerical modeling

Numerical modeling has been around for more than 20 years and has proven to be an effective tool to simulate the behavior of the stresses that act on mine pillars. The advantage that numerical modeling has over field testing is that it is less time consuming and more cost effective. Normally a numerical model is calibrated with field testing data, to ensure proper and accurate results. There are three types of numerical methods: continuous, discrete, and hybrid. The Boundary Element Method (BEM), Finite Element Method (FEM), and Finite Difference Method make up continuum models. The discrete element method (DEM) and the discrete fracture network (DFN) are examples of discrete numerical models. Continuum and discrete modeling are combined in hybrid numerical modeling. The aim and of the numerical study will determine which numerical approach to use. Continuum models are typically used for rockmass that are huge and highly deteriorated or when the rockmass has no significant fractures. Discrete models are used when the fractures have a significant effect on rock movement (Jing & Hudson, 2002).

2.2.1.1 Numerical modeling overview

When compared to other continuum methods, the BEM has the advantage of a reduced computational time for rockmass modeling as well as a simpler mesh generation and input data preparation. The BEM can also be used to simulate rock fracturing, but in most cases

it is limited to fracturing in uniform and linear elastic bodies (Jing & Hudson, 2002). Examples of BEM programs are Examine 2D and Map3D. There are three BEM approaches that are significant for rockmass modeling: direct method, indirect method, and displacement discontinuity method.

- The Direct Method entails directly solving stresses and displacements from specific boundary conditions.
- The Indirect Method consist of determining the stresses at boundaries at the start followed by determining displacements with the help of 35 independent relationships.
- The Displacement Discontinuity Method is appropriate for modeling the fracture growth and is used for rock fracture challenges.

The idea behind the finite element method (FEM) is to break the problem region into smaller sections known as finite elements, do local calculations inside each finite element, and then execute finite element assembly to get the answer to the global matrix equation. The FEM was the first numerical technique to take into consideration boundary conditions, nonlinearity, complex geometries, and material heterogeneities (Jing & Hudson, 2002). Examples of FEM software are PLAXIS 3D, Rocscience RS2 and RS3.

The main method of the FDM is to discretize partial differential equations by substituting differences specified over a predetermined time in the coordinate direction for partial derivatives (Jing & Hudson, 2002). Three techniques are used by FDM: the core difference approach, implicit or backward, and explicit or forward. FLAC3D is an example of FDM software.

DEM is a collection of stiff or deformable blocks/elements used to calculate contact forces by continually updating the entire deformation operation to reflect an acceptable constitutive model. The DEM is primarily based on implicit and explicit formulations of equations of motion of rigid or deformable structures. DEM software examples include UDEC and Itasca's 3DEC, which are two-dimensional and three-dimensional models (Jing & Hudson, 2002).

2.2.1.2 Numerical modeling application

Hoek & Brown, (1980) used FEM to study rock pillars and to characterize the stresses induced in them. They determined that at mid-height, the pillar resulted in a constant stress distribution for thin pillars. The stress examined at the center of the pillar corresponds to the uniaxial compressive strength and can be expressed as: the maximum principal stress (σ_1) equals the average external stress and the minimum principal stress is zero.

Kaiser and Tang (1998) formulated a Rock Failure Process Analysis (RFPA) FEM code and subsequently conducted a failure analysis on rib pillars to simulate the collection and release of seismic energy. They discovered a link between stress, strain, acoustic and seismic energy release. Kaiser and Tang (1998) also determined that the pillar carrying capability falls dramatically with weak hanging or footwall, resulting in seismicity arising at far lower stress levels than anticipated.

Maybee (2000) utilized Examine2D and Map3D (BEM code) to reproduce the hard rock pillars and estimate the stress on the pillars in order to evaluate it using the tributary area theory. According to the study, 13 pillars in a row must be modeled in order to effectively depict stresses in a room and pillar mine on a two-dimensional plane.

Esterhuizen (2006) performed numerical studies on limestone mine pillars using FLAC3D and found that the failure of hard rock pillars was brittle with aspect ratios less than 1 when passing through the center of the 39 pillars. If the aspect ratio is greater than one it would lead to ribs spalling (brittle) followed by shear failure within the pillar, shown in Figure 2.4. A hard rock pillar with a discontinuity was also modeled to investigate the effect of geological structure on the pillar. It was discovered that it reacted similarly to a fracture plane in a rock sample.

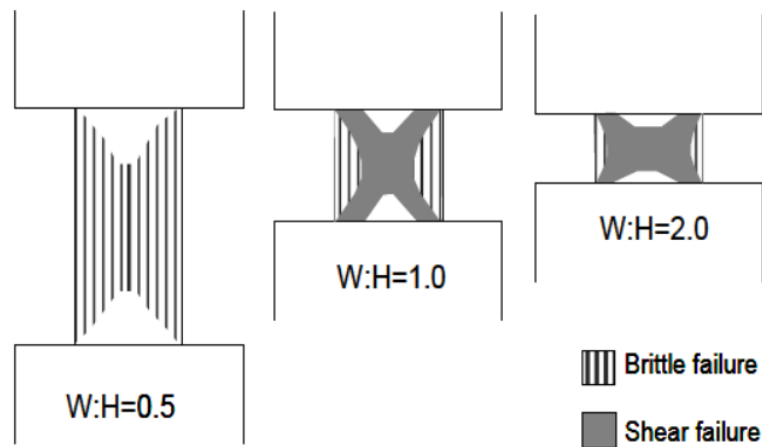


Figure 2.4: Brittle and shear failure modes in pillars (Esterhuizen, 2006).

Hedley et al. (1984) performed a stress evaluation on two pillars with same extraction ratio. One pillar was a horizontal pillar that was experiencing normal loading while the other pillar was a 20° inclined pillar where it underwent oblique loading. The study showed that at similar stress, the horizontal pillar was stable whereas in the inclined pillar, the failure extended from the top corner of the one side to the bottom corner of the opposite side, shown in Figure 2.5. The numerical investigation concluded that the inclined pillars in the Quirke Mine created the chain pillar burst phenomenon.

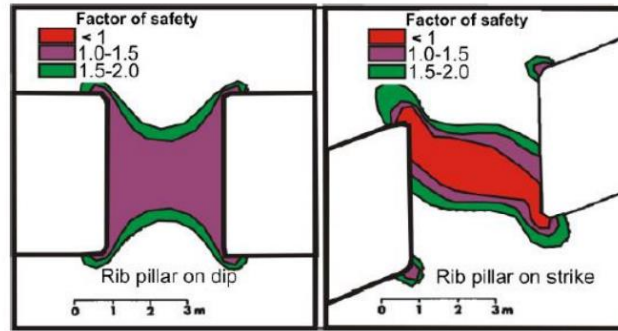


Figure 2.5: Pillars subjected to normal loading and oblique loading (Hedley et al., 1984).

Elmo and Stead (2010) used the hybrid numerical model ELFEN to create a series of two-dimensional pillar models with joints. They discovered that shear sliding failure occurs when inclined joints dip at a greater angle than the friction angle of the joint, but vertical joints and joints dipping below the friction angle of the joint suggest splitting failure. Lower joint stiffness was also associated with more precise pillar mechanical response, including discrete block movement, lateral spalling, and pillar core fracturing.

According to Suorineni et al. (2011), as the orebody is subjected to oblique loading scenarios, it is more prone to generate rock bursts. Suorineni et al. (2013) used Phase2D to perform a stress evaluation on pillars under oblique loading circumstances. It was established that the direction of the primary far-field principal stresses relative to pillar strike or dip can also affect rock bursts. The stress distribution in the pillar is shown in Figure 2.6 when the far-field principal stresses are positioned at an angle to the pillar.

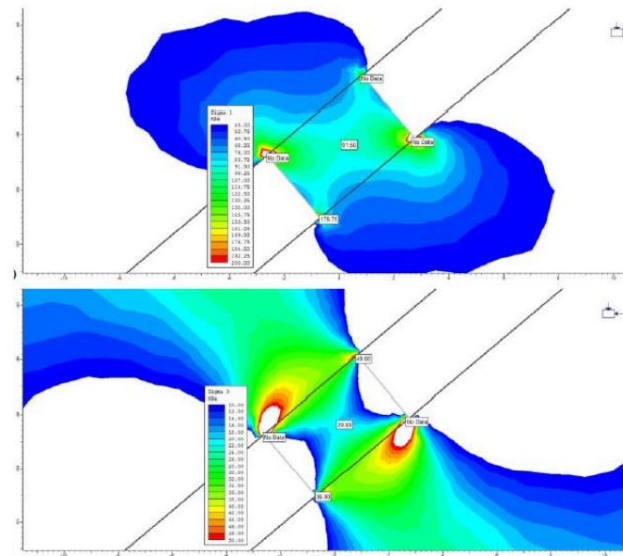


Figure 2.6: Stress distribution in the pillar when the far-field principal stresses are oriented at an angle to the pillar (Suorineni et al., 2011).

2.2.2 Analytical methods

Before any underground mining activity occurs the stresses in an underground rockmass are known as virgin or natural or in-situ stresses. These virgin stresses can be of gravitational, tectonic or residual type. This section describes a very common and simplified analytical method to determine the in-situ stresses. The virgin vertical stress (σ_v) is due to gravitational loading acting on the overlying strata and can be obtained as:

$$\sigma_v = \gamma h$$

where:

σ_v = vertical stress, MPa

γ = unit weight of rockmass, MN/m³ and

h = depth of cover, m.

The horizontal stresses (σ_h) associated to the virgin vertical stresses can be express as follows:

$$\sigma_h = k\sigma_v$$

Where:

k = is the relation between the horizontal to vertical stress and is dependent on the stress field.

The value of k due to overburden stress in elastic rock behavior, assuming no displacement is occurring, is:

$$k = \frac{\nu}{(1 - \nu)}$$

where:

ν = Poisson's ratio

For most rocks the Poisson's ratio changes between 0.15 to 0.35, with a general value of 0.25 (Foroughi, 1996).

The most used analytical theory to calculate pillar load is the tributary area method. This method can only be used when you have regular spaced, square, or rectangular pillars.

2.2.2.1 Tributary area method for horizontal seams

The Tributary area theory has been described in numerous textbooks (Bieniawski, 1984; Herget, 1988; Peng, 1986). As illustrated in Figure 2.7, the technique accepts that each pillar carries the weight above it as well as one-half of the width of the rooms or entry on all sides of the pillar. For a square room and pillar pattern the average pillar stress (σ_p) can be calculated as follows:

$$\sigma_p = \gamma h \frac{(w + B)(L_p + B)}{wL_p}$$

where:

σ_p = average pillar stress, MPa

γ = unit weight of the surrounding rocks, MN/m³

h = depth below surface, m

w = pillar width, m

L_p = pillar length, m and

B = entry width, m.

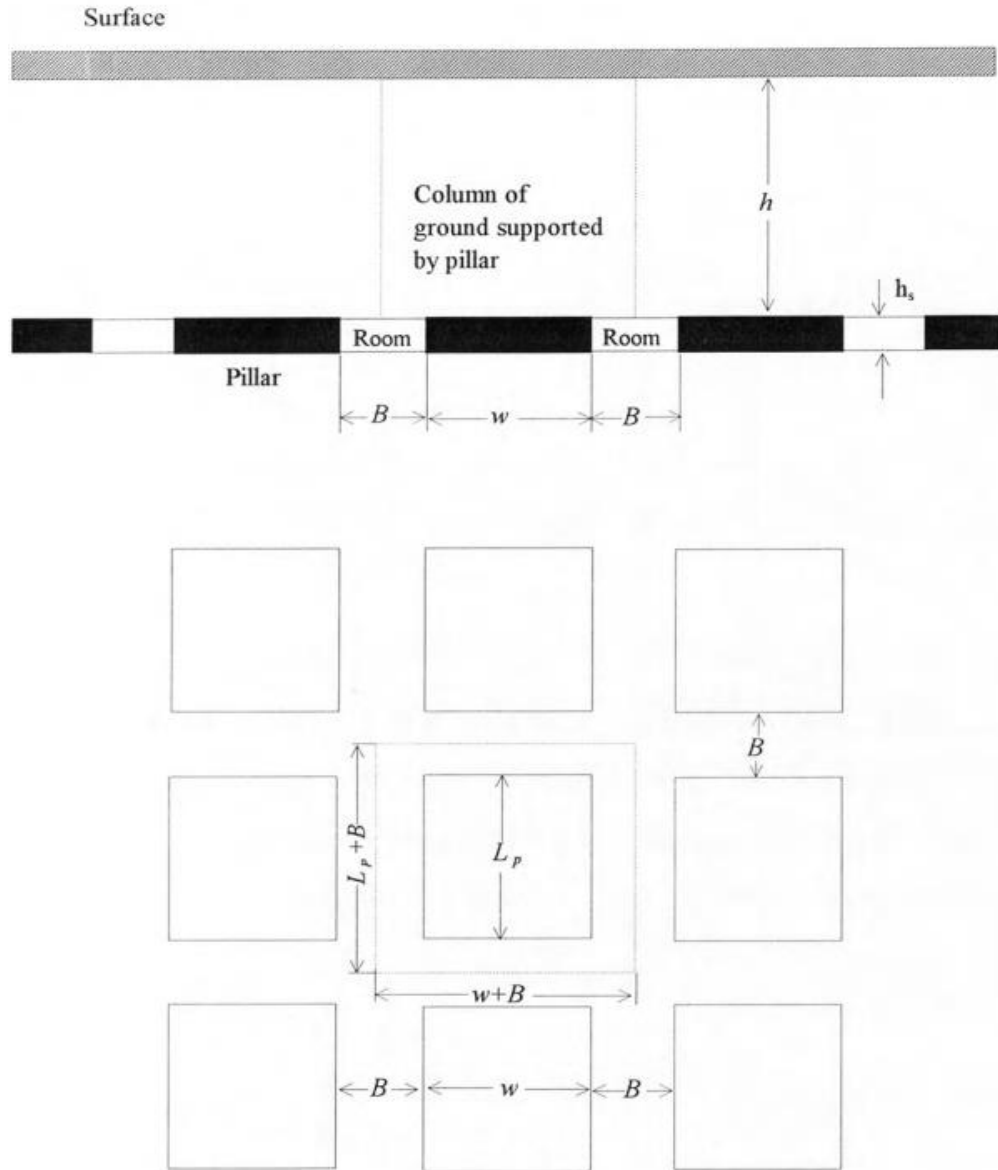


Figure 2.7: Tributary method explained for a room and pillar mining layout (Foroughi, 1996).

The extraction ratio (R) is the ratio of the mined-out area to the total area and can be determined as follows:

For rectangular pillars:

$$R = 1 - \left[\frac{w}{w + B} \right] \left[\frac{L_p}{L_p + B} \right]$$

For square pillars:

$$R = 1 - \left[\frac{w}{w + B} \right]^2$$

2.2.2.2 Tributary area method for inclined seams

Although tributary area approach is a common method for determining pillar stresses due to its simplicity (Bieniawski, 1983), the presence of shear stresses in dipping coal seams complicates matters. The. Some authors (Jeremic, 1985; Pariseau, 1982; Sheorey, 1993; Trumbachev & Melnikov, 1964) have used the tributary area approach to estimate the pillar load in inclined coal seams. Figure 2.8 and Figure 2.9 show the forces that act on inclined pillars.

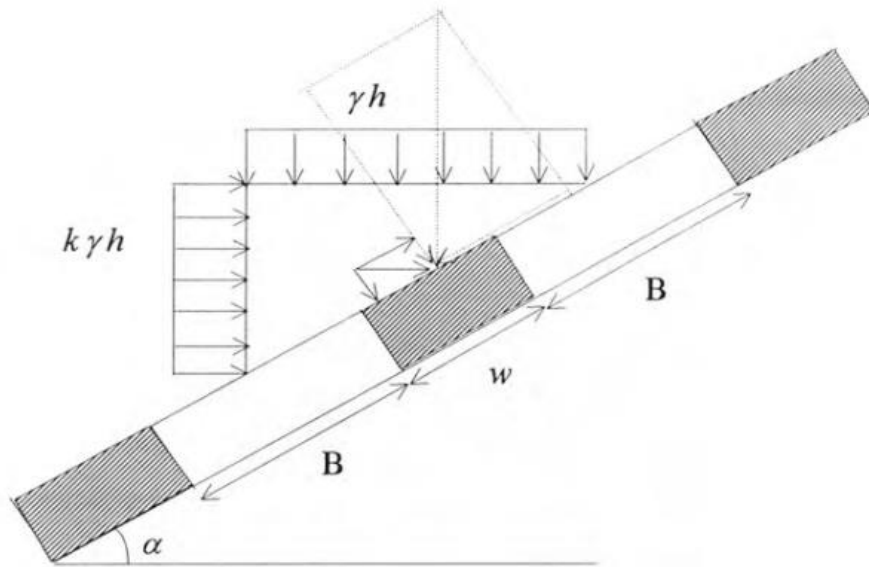


Figure 2.8: Inclined seam with pillar ribs perpendicular to the roof (Foroughi, 1996).

The following equations describe how to calculate the normal stress (σ_n), shear stress (τ_t), average pillar stress (σ_p) and the average shear stress in the pillar (τ_p) in inclined coal seams (Foroughi, 1996).

$$\sigma_n = \gamma h (\cos^2 \alpha + k \sin^2 \alpha)$$

$$\tau_t = \gamma h \left(\frac{k - 1}{2} \right) \sin 2\alpha$$

$$\sigma_p = \frac{\sigma_n}{1 - R} = \sigma_n \left(\frac{B + w}{w} \right)^2$$

$$\tau_p = \frac{\tau_t}{1 - R} = \tau_t \left[\frac{B + w}{w} \right]^2$$

where

γ = unit weight of overburden, MN/m³

h = depth of seam, m

k = ratio of the horizontal to vertical in-situ stress

α = seam inclination

R = extraction ratio

w = least pillar width, m and

B = width to mined out stope, m.

Foroughi (1996) established that the shear and normal stresses are affected by the seam inclination and the horizontal to vertical in-situ stress ratio. When k is less than one, the shear stresses are at their highest when the seam inclination is 45° and lowest when the seam inclination is 0° or 90°. To reduce shear stresses in an inclined pillar, leave the pillar with the pillar axis inclined up dip by a specific angle (β_1), as indicated in Figure 2.9.

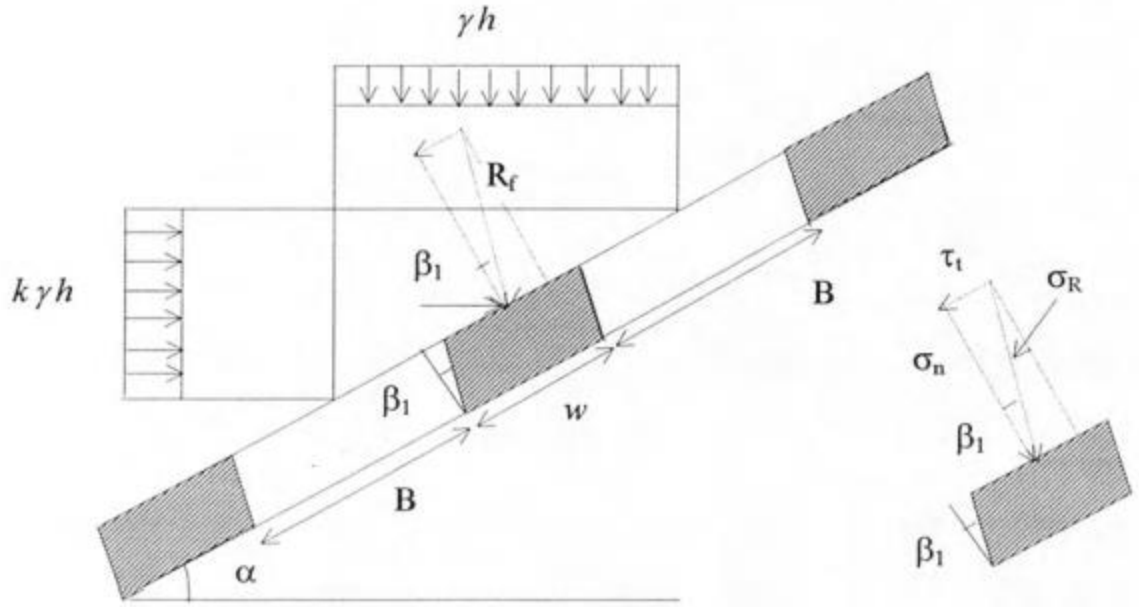


Figure 2.9: Inclined seam with deviating pillar rib angles (Foroughi, 1996).

The most effective value for β_1 can be obtained from the state that the resultant stress acts along the pillar. The angle β_1 depends upon the seam inclination and k . This can be defined by using the following equations:

$$\tan(\beta_1) = \frac{\tau_t}{\sigma_n}$$

$$\sigma_n = \gamma h (\cos^2 \alpha + k \sin^2 \alpha) = \gamma h \left[\frac{k + 1 + (1 - k) \cos 2\alpha}{2} \right]$$

$$\tau_t = \gamma h \frac{(k - 1) \sin 2\alpha}{2}$$

$$\tan \beta_1 = \frac{(k - 1) \sin 2\alpha}{k + 1 + (1 - k) \cos 2\alpha}$$

$$R_f = k \gamma h (B + w) \frac{\sin \alpha}{\cos \alpha}$$

where:

β_1 = angle of pillar axis deviation

σ_n = normal stress, MPa

τ_t = shear stress, MPa

γ = unit weight of overburden, MN/m³

h = depth of the seam, m

k = ratio of the horizontal to vertical in-situ stress

α = seam inclination

R_f = resultant stress, MPa

2.2.2.3 Limitations of using the tributary method

Although the tributary area method simplifies calculations, it does have certain drawbacks. The approach assumes that the overburden load is evenly spread over the pillars and ignores the presence of abutments in a mining area, which results in differing stress distributions (Maritz, 2015). The tributary area technique solely takes into account the pre-mining component of normal stress, which acts in the same direction as the primary axis of the pillar support system. Other components of pre-mining stress, according to the idea, are insignificant and have no effect on the pillar's stability (Brady & Brown, 2006).

2.2.3 Other methods

There are also other methods available in literature to calculate pillar stress. The empirical methods are built on equations obtained from databases of various case studies. These empirical methods have been validated for different regions and are widely used in the mining industry (Tuncay et al., 2021). One drawback of the utilization of empirical methods is that they can only be applied in situations similar to those under which they were developed (Esterhuizen et al., 2008).

Discussion

Throughout the literature there are various ways of estimating pillar stress, more specifically inclined pillar stress. The shear forces found in dipping coal seams reduce the pillars' stability. When the seam inclination is between 30 and 60 degrees and the pillar axis is normal to the stratification, shear stresses are at a maximum (Foroughi, 1996). It is acceptable to leave the pillars with a deviation angle of π , so that the stress distribution is similar to that of a modest dip, to reduce shear stresses. The tributary area is the most extensively used analytical method for approximating pillar stress, however it has several drawbacks. Numerical modeling has also been used by many authors on how to determine inclined pillar stress.

2.3 Intact rock strength

The strength of the intact rock block material is defined by intact rock strength, which governs the strength of the rockmass. Igneous and metamorphic rocks can mostly be classified as brittle. This implies an abrupt decrease in strength when a limiting stress level is surpassed. Weak sedimentary rocks can fail in a more ductile manner. This means that when the limiting stress is surpassed there is no too little reduction in strength.

Most of the information gained on intact rock strength came from laboratory testing, such as the uniaxial tensile strength (UTS) test, unconfined compressive strength (UCS) test, and the triaxial compressive strength (TXL) test. There are various papers available on these testing methods, the reliability and the source of errors involved in the testing Bertuzzi (2019). In rock mechanics and underground design there is a need for a mathematical expression (or criteria) to model the strength of rock under different stresses. The most adopted rock mechanics failure criteria include Mohr-Coulomb, Griffith, Drucker-Prager, Wiebols-Cook, Hoek-Brown, extension strain, Bieniawski, Lade, Christensen and You. For the purpose of this study only the Mohr-Coulomb and the Hoek & Brown failure criteria are discussed.

2.3.1 Mohr-Coulomb failure criterion

The most basic and widely used failure criterion in rock mechanics is the Mohr-Coulomb criterion. This strength criterion accepts that the failure occurs on a plane due to the shear stress (τ) on that plane which at failure is a function of that plane's cohesion (c), friction angle (ϕ) and the normal stress (σ_n) acting on that plane.

$$\tau = c + \sigma_n \tan \phi$$

Where the cohesion and the friction angle are linked to the unconfined compressive (σ_c) and tensile strengths (σ_t) as:

$$\sigma_c = \frac{2c \cos \phi}{1 - \sin \phi}$$

$$\sigma_t = \frac{2c \cos \phi}{1 + \sin \phi}$$

Principal stresses are another way to express the Mohr-Coulomb criterion.:

$$\sigma_1 = \frac{2c \cos \phi}{1 - \sin \phi} + \sigma_3 \left[\frac{1 + \sin \phi}{1 - \sin \phi} \right]$$

or

$$\sigma_1 = \sigma_c + k \sigma_3$$

The Mohr-Coulomb failure criterion is appropriate to use when analyzing the shear strength of planar features such as joints and other discontinuities. However, it is limited

to analyze the peak rock strength because the actual peak strength envelopes are normally non-linear and it implies that failure occurs as shearing in the direction $\frac{\pi}{4} + \frac{\phi}{2}$.

2.3.2 Hoek & Brown failure criterion

The Hoek-Brown empirical failure criterion was created from a best-fit curve to experimental failure data plotted in $\sigma_1 - \sigma_3$ space. The goal was to develop a simple, empirical rock failure criterion that sufficiently explains the reaction of an intact rock sample to uniaxial tensile stress, triaxial compressive stress, and triaxial compressive stress. The criterion has a large uniaxial compressive stress (σ_c) intact rock data set, that ranges from 40 – 580 MPa (Hoek and Brown 1980).

$$\frac{\sigma_1}{\sigma_c} = \frac{\sigma_3}{\sigma_c} + \sqrt{m \frac{\sigma_3}{\sigma_c} + s}$$

Where σ_3 is the confinement stress, s is a rockmass constant ($s=1$ for intact rock, $s<1$ for broken rock), and m is a constant that is characteristic of the rock type (typical values range from 25, for coarse grained igneous rock and metamorphic rocks to 7 for carbonated rocks). A general Hoek & Brown criterion was later introduced was introduced by Hoek et al. (2002) that made the parameter a variable between 0.5 and 0.65 for rockmass failure.

$$\sigma_1 = \sigma_3 + \sigma_{ci} \left[m_b \frac{\sigma_3}{\sigma_c} + s \right]^a$$

Where m_b denotes a decreased value of the material constant m_i and is provided by:

$$m_b = m_i \exp \left[\frac{GSI - 100}{28 - 14D} \right]$$

s and a are constants for the rockmass given by the following equations:

$$s = \exp \left[\frac{GSI - 100}{9 - 3D} \right]$$

$$a = \frac{1}{2} + \frac{1}{6} (e^{-GSI/15} - e^{-20/3})$$

D is a factor that depends on the amount of disruption caused by blast damage and stress relaxation on the rockmass. It ranges from zero for undisturbed in-situ rockmass to one for highly disturbed rockmass.

2.3.3 Mohr-Coulomb vs Hoek & Brown failure criteria

In geotechnical engineering, the Hoek & Brown failure criterion is the most often employed rockmass failure criterion. To assess rockmass properties, the criterion combines the geological strength index (GSI) and intact rock parameters (Saeidi et al., 2022). When focusing on the stability of soil slopes, the use of the Mohr-Coulomb (MC) failure criterion

is a standard technique. Even if the Hoek-Brown (HB) failure criterion proved to be more appropriate for evaluating a rockmass, the Mohr-Coulomb model is still widely used in the stability study of rock slopes. This could be because the factor of safety can be simply stated in terms of basic shear strength characteristics like cohesion and angle of internal friction (Poklopová et al., 2021).

There are inherent shortcomings in the simplicity in the Mohr-Coulomb failure criteria. The first flaw is that the Mohr-coulomb failure criteria is developed for soil slopes, and it assumes that the soil will fail in shear. The tensile strength is not well described or explained in the equations. This shortcoming is not too serious when applying the Mohr-Coulomb failure criteria for rocks since, when dealing with rocks only the compression region is focused on and not the tension region. The second shortcoming in the Mohr-Coulomb failure criteria is that it assumes a linear failure envelope. The failure envelope of many rocks is nonlinear and the Mohr-Coulomb failure criteria can overestimate the shear strength for rocks (Fahrman, 2016).

Both approaches assume different rockmass yield and deformation characteristics. As demonstrated in Figure 2.10, the Hoek and Brown model assumes an elastic-brittle-plastic rockmass behavior, whereas the Mohr-Coulomb model assumes an elastic-perfectly-plastic rockmass behavior. The outcomes of the two models will be identical until the point of failure. For the same stress, the Hoek & Brown model will exhibit greater plastic straining than the Mohr-Coulomb model after failure (Saiang et al., 2014).

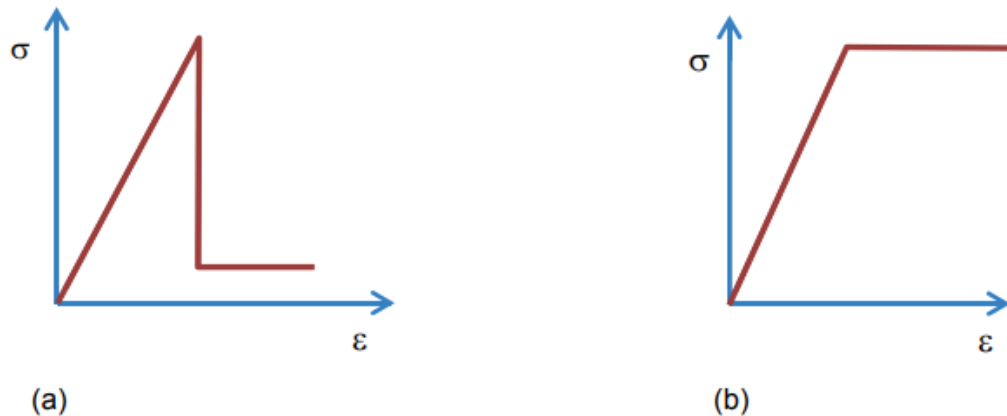


Figure 2.10: (a) shows a Hoek & Brown elastic-brittle-plastic rockmass behavior and (b) a Mohr-Coulomb elastic-perfectly-plastic rockmass behavior (Saiang et al., 2014).

Discussion

There are various failure criteria available in the literature, but the most common are the Hoek & Brown and the Mohr-Coulomb failure criteria. The Mohr-Coulomb failure criteria was mainly developed for soil slopes while the Hoek & Brown failure criteria was developed for rockmass. For plastic behavior the Hoek & Brown model and the Mohr

Coulomb models behave similar. After failure larger strains are observed in the Hoek & Brown models (Saiang et al., 2014).

2.4 Pillar strength

Pillar strength can be defined as the maximum resistance of a pillar to axial compression. According to York et al., (2000) the in-situ strength of the rockmass is the primary strength factor of a pillar, but there are also other factors that should be taken into consideration when deriving the strength of a pillar. These factors are:

- Jointing within the pillar
- Roof and floor conditions
- Seam dip
- Total system loading
- Virgin horizontal and vertical stress ratio (k-ratio)
- Creep
- Length to width ratio
- Pillar dimensions

Most of the current pillar strength equations do not take the above-mentioned factors into account. This means that when one of these factors becomes dominant, inaccurate strength results may be obtained. Any difference of the above-mentioned factors from the current empirical range must be given specific attention in order to yield more accurate results.

2.4.1 Horizontal pillars

A number of equations have been established to determine the strength of pillars in coal and hard rock mines. Table 2.2 presents several pillar strength equations that have been developed by different researchers around the world. Most of the strength equations in Table 2.2 are related to coal pillars (Das et al., 2019) and were developed through laboratory compression tests, large scale in-situ tests, analytical solutions, collapsed and stable pillar cases, and numerical modeling for coal mines. Due to the complexity of the rockmass and the problems encountered in evaluating the strength of the in-situ rock, a simplified approach is usually used to determine the strength of a pillar. It should be noted that these equations work best in situations similar to those that they were derived for (Das et al., 2019).

Table 2.2: Several pillar strength equations

No	Authors	Equation	Derivation	Coal pillar/ Rock pillar	Width to height	Type of strength employed
1	Greenwald et al. (1941)	$s = 0.67k \frac{w^{0.5}}{h^{0.88}}$	In-situ test	Coal	Slender	In-situ size 30 cm
2	Gaddy (1956)	$s = k \frac{w^{0.5}}{h}$	Lab test	Coal	Slender	Lab size 25 cm
3	Obert & Duvall (1967)	$s = k(0.78 + 0.22 \frac{w}{h})$	Lab test	Coal	Slender	In-situ size 'critical'
4	Salamon & Munro (1967)	$s = 7.2 \frac{w^{0.46}}{h^{0.66}}$	Pillar Cases	Coal	Slender	Constant strength
5	Salamon & Munro (1967) generalized	$s = 0.79k \frac{w^{0.46}}{h^{0.66}}$		Coal	Slender	In-situ size 30 cm
6	Hedley & Grant, (1972)	$s = k \frac{w^{0.5}}{h^{0.75}}$	Empirical	Rock		
7	Bieniawski (1968)	$s = k \left(0.64 + 0.36 \frac{w}{h} \right)$	In-situ test	Coal	Slender	In-situ size 'critical'

No	Authors	Equation	Derivation	Coal pillar/ Rock pillar	Width to height	Type of strength employed
8	Bieniawski (modified) Logie & Matheson (1982)	$s = k \left(0.64 + 0.36 \frac{w}{h} \right)^{1.4}$	In-situ test	Coal	Squat	In-situ size 'critical'
9	Lunder & Pakalnis, (1997)	$s = 0.44\sigma_c(0.68 + 0.52k)$	Empirical	Rock	Both	
10	Salamon & Wagner (1985)	$s = 0.79k \frac{R^{0.46}}{V^{0.66}} \left\{ \frac{0.59}{\varepsilon} \left[\left(\frac{R}{R_0} \right)^\varepsilon - 1 \right] + 1 \right\}$ <p>Where, R_o = is the critical w/h=5, R=w/h of pillar, V= is the pillar volume, ε =is a constant = 2.5 (proposed)</p>	Case studies and theoretical analysis	Coal	Squat	In-situ size 30 cm
11	Wilson (1972)	<p>Case I $w > 2\bar{x}$</p> <p>(Wilson's equations are all in tonne, ft units.)</p> <p>Rectangular pillars</p> $s = \frac{4\gamma H}{w_1 w_2} [w w_1 - 1.5(w + w_1)hH \times 10^{-3} + 3h^2 H^2 \times 10^{-6}]$ <p>Long pillars</p>	Theoretical analysis	Coal	Both	No strength

No	Authors	Equation	Derivation	Coal pillar/ Rock pillar	Width to height	Type of strength employed
		$s = \frac{4\gamma H}{w} (w - 1.5hH \times 10^{-3})$ <p>Case II $w \leq 2\bar{x}$</p> <p>Rectangular pillars</p> $s = 667\gamma \frac{w}{w_1 H} \left(w_1 - \frac{w}{3} \right)$ <p>Long pillar</p> $s = 667\gamma \frac{w}{H}$ <p>$\bar{x} = 0.0015hH$ is the failed coal zone</p> <p>$\gamma = 0.0707 \text{ t/ft}^2$ is the rock density</p>				
12	Wilson (1983)	<p>Case I Roadways stable</p> $s = \frac{1}{ww_1} \int_{qp}^{q\gamma H} (w - 2x)(w_1 - 2x) d\sigma + qp$ $+ \frac{\sigma_o}{ww_1} (w - 2x)(w_1 - 2x)$ <p>Case 2 Roadways unstable</p>	Theoretical analysis	Coal	Both	In-situ strength = (lab strength)/5

No	Authors	Equation	Derivation	Coal pillar/ Rock pillar	Width to height	Type of strength employed
		$s = \frac{1}{ww_1} \int_{qp}^{\sigma'} (w - 2x)(w_1 - 2x) d\sigma + qp$ <p>Where $\sigma' = qp \left(\frac{w}{h} + 1 \right)^{q-1}$ or $qp \exp \left(\frac{wF}{2h} \right)$</p> <p>$\sigma_0$ = is the in-situ strength, p = is a constant for broken coal = 0.1 MPa (recommended), q = triaxial constant = 3.5 (average recommended)</p> <p>These equations are subject to the two ground conditions listed below:</p> <p>Yield in roof, seam, and floor</p> $x = \frac{h}{2} \left[\left(\frac{\sigma}{qp} \right)^{\frac{1}{q-1}} - 1 \right];$ $\bar{x} = \frac{h}{2} \left[\left(\frac{\gamma H}{p} \right)^{1/(q-1)} - 1 \right]$ <p>Yield in seam, rigid roof, and floor</p> $x = \frac{h}{F} \ln \frac{\sigma}{qp}; \bar{x} = \frac{h}{F} \ln \frac{\gamma H}{p}$				

No	Authors	Equation	Derivation	Coal pillar/ Rock pillar	Width to height	Type of strength employed
		<p>Where</p> $F = \frac{q-1}{\sqrt{q}} + \frac{(q-1)^2}{q} \tan^{-1} \sqrt{q}$ <p>\tan^{-1} in radians</p>				
13	Sheorey et al. (1986)	$s = 0.66kh^{-0.35} + 6.3 \left\{ K\gamma H \left[1 - \exp \left(-\frac{1.5w}{D} \right) \right] \right\}^{0.8}$ <p>Where $D = 25 + 0.1H$, $K =$ virgin horizontal – vertical stress ratio</p>	Theoretical empirical method, and case studies	Coal	Both	In-situ size 30 cm
14	Sheorey et al. (1987)	$s = 0.27k \frac{w^{0.5}}{h^{0.86}}$	Case studies	Coal	Slender	Lab size 25 cm
15	Sheorey et al. (1987)	$s = 0.27kh^{-0.36} + \frac{H}{160} \left(\frac{w}{h} - 1 \right)$	Theoretical, empirical method, and case study	Coal	Both	Lab size 25 cm
16	Sheorey (1992)	$s = 0.27kh^{-0.36} + \left(\frac{H}{250} + 1 \right) \left(\frac{w}{h} - 1 \right)$	Theoretical, empirical method, and case study	Coal	Both	Lab size 25 cm

No	Authors	Equation	Derivation	Coal pillar/ Rock pillar	Width to height	Type of strength employed
17	Van der Merwe (1999)	$s = 4 \frac{w^{0.81}}{h^{0.76}}$	Case studies	Coal		Constant strength
18	Van der Merwe (2003)	$s = k \frac{w}{h} (k = 2.8 - 3.5)$	Case studies	Coal		Constant strength

The variables are as follow: s is the pillar strength (MPa), w is the width of the pillar or long pillar or smaller width of rectangular pillar (m), w_1 is the longer width of a rectangular pillar (m), H is the depth of cover (m), and s is the strength of coal (MPa) both in-situ or laboratory conditions.

Most of the pillar strength equations that are shown in Table 2.2, incorporates the strength and geometric parameters of a pillar, but fails to include the seam inclination effect. Due to the complex behavior of the inclined coal seam, pillar strength equations in Table 2.2 cannot be applied to inclined pillars (Mgumbwa et al., 2010). The pillar attempts to slide alongside the contact planes towards the real dip on an inclined seam. This increases the likelihood of shear failure in the inclined pillar as well as separation from the roof and floor contact points. The stresses at the pillar-to-rock contact are determined by the friction angle and cohesiveness of the contact planes, as well as the rock mass's deformation characteristics. Despite the fact that it is not typically taken into account in pillar strength calculations, seam inclination is crucial in determining the sliding of the coal pillar along the overlaying and underlaying contact surfaces (Das et al., 2019).

If these equations are adopted in situations where they are not intended for, the pillar strengths can be overestimated resulting in pillar failure (Garza-Cruz et al., 2019). A study done by Maritz (2015), indicated that various platinum mines in South Africa, which have steep dipping orebodies, have adopted the Hedley & Grant (1972) equation for hard rock mining, which resulted in pillar failure. Lorig & Cabrera (2013) also indicated that the empirical strength curves are not helpful in the case of inclined pillars, since they do not account for the pillar inclination and width to height ratios of more than 2.

2.4.2 Inclined pillars

Throughout the literature several authors have tried to estimate the strength of inclined pillars. The techniques identified to estimate inclined pillar strength are analytical solutions, laboratory testing and numerical modeling.

2.4.2.1 Analytical solutions

Pillar strength formulae used around the world are designed for horizontal coal pillars. Das et al. (2019) created an analytical approach for estimating the strength of square, rectangular, and extremely long coal pillars. The analytical solutions can be used for both inclined and horizontal coal pillars. The mathematical solutions were developed in order to calculate the confining stress in the coal pillar, which was then employed in the Sheorey (1997) rockmass failure criterion to calculate the peak stress in the pillar at the time of collapse. The intact and the broken coal properties are required as input parameters for the mathematical models and can be obtained through laboratory testing. The mathematical solutions also take into consideration the shearing effect when the dip of the coal seam increases. At the roof-pillar and floor-pillar interface, a Mohr-Coulomb criterion was considered for the shearing effect. It was observed that the mathematical solutions worked when tried to predict stable and failed cases of flat and inclined pillars.

2.4.2.2 Laboratory testing

Jessu et al. (2018) conducted a laboratory study on gypsum and sandstone to see how inclination affects the strength reduction. Gypsum and sandstone are representatives of brittle rock, and have lower strengths, making them suitable for laboratory testing. PVC tubes with inner diameters of 50 mm were used for the gypsum, while PVC tubes with inner diameters of 42 mm were utilized for the sandstone. PVC mold tubes were cut perpendicular to the tube length to replicate horizontal pillars, and at an angle for both ends to simulate inclined pillars. 65 Gypsum tests and 27 sandstone tests were done with width to height ratios of 0.4, 0.5, 1.0, 1.5 and 2.0. Platens were manufactured and used in the UCS test at 10° and 20° to simulate the drip effect. Figure 2.11 shows the results of the gypsum and the sandstone after the Uniaxial Compressive Strength (UCS) test was done. The percentage reduction in strength of the samples for all the width to height ratios were similar. The strength reduction for gypsum at 10° and 20° was respectively 76%-79% and 54%-59%. The strength reduction for sandstone at 10° and 20° was respectively 67%-72% and 42%-47%.

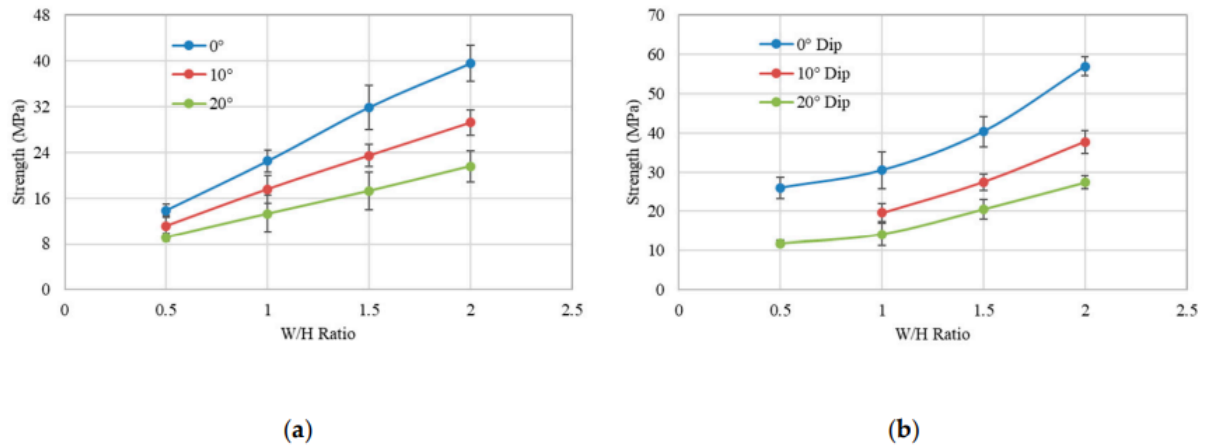


Figure 2.11: The strength change of the (a) gypsum samples, (b) sandstone samples for various width to height ratios and various inclinations (Jessu et al., 2018).

Figure 2.12: Strength reduction for gypsum and sandstone (derived from Jessu et al., 2018) Figure 2.12 was derived from Figure 2.11 (which was published by Jessu et al., 2018) in order to better illustrate how the strength decreases as the inclination increases, for the gypsum and the sandstone.

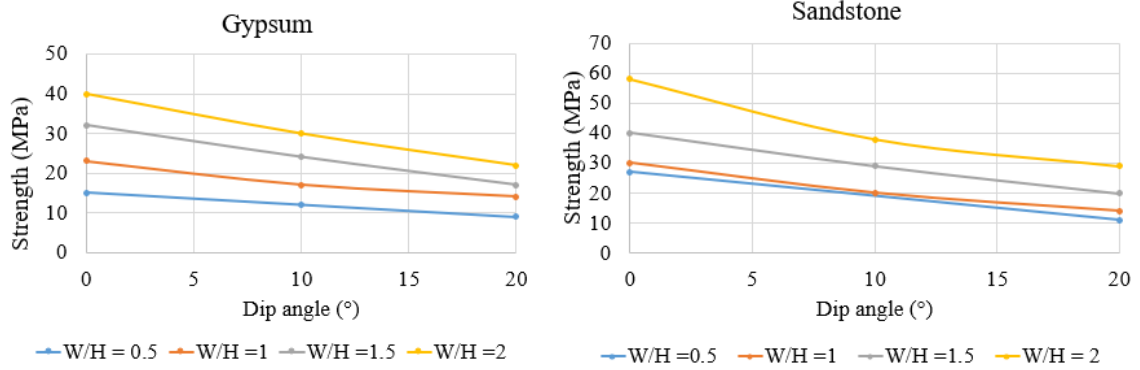


Figure 2.12: Strength reduction for gypsum and sandstone (derived from Jessu et al., 2018)

Luo et al. (2020) presented a similar study where 112 molds of a mixture of Portland cement and gypsum were made. The molds had width to height ratios of 1.0, 1.5, and 2.0. Figure 2.13a shows the two cushion blocks with inclinations of 10° and 20° used to simulate the dip effect. The results of the UCS test are shown in Figure 2.13b. The authors found that the reduction in strength of the samples for all the width to height ratios were similar.

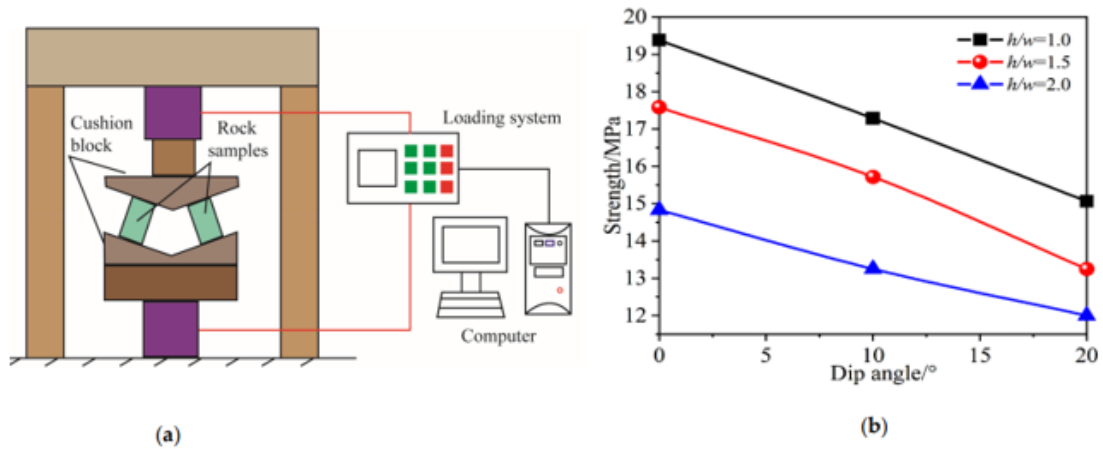


Figure 2.13: Shows (a) the cushion blocks used in the experimental setup, and (b) the UCS results (Luo et al., 2020).

In both cases, Jessu et al. (2018) and Luo et al. (2020), the results of the UCS tests showed that when the dip angle increases, the strength of the pillar decreases. Laboratory testing can be helpful to determine the strength reduction factors. Strength reduction factors can therefore lead to a better design of inclined pillars without overestimating the stability factor.

2.4.2.3 Numerical solutions

Numerical modeling is an effective method for addressing complicated geological problems through the computational simulation of geological processes. For example, numerical modeling can solve complex stress scenarios in an underground mine without the need for experimental laboratory setups. However, before numerical modeling can be done, the model must be calibrated according to site-specific data.

Suorineni et al. (2013) used numerical analysis to better understand the behavior of inclined pillars. They found that inclined orebodies are more likely to fail since the inclined pillars lose their strength due to a loss in confinement. The loss of confinement increases with pillar inclination, pillar width-to-height ratio and the k -ratio (the ratio between the horizontal principal stress to the vertical principal stress).

Jessu et al. (2018) investigated the strength performance of inclined pillars using laboratory and numerical investigations. Before any inclined pillar modeling could be done, the model was calibrated. The results were compared to those of Lunder and Pakalnis (1997). Jessu et al. (2018) simulated pillars at five different inclinations of 0° , 10° , 20° , 30° and 40° . The advantage that the numerical model has over the laboratory results is that numerical modeling could be used to study five different inclinations, while laboratory experimentation could only study two inclinations. As a result of the numerical modeling approach, an equation was proposed for strength reduction factors that would need to be applied to each different inclination. The strength reduction factors for inclinations 10° , 20° , 30° and 40° were found to be 0.94, 0.87, 0.78 and 0.67. Thus, strength reduction factors can be used to estimate the strength of inclined pillars.

Garza-Cruz et al. (2019) presented a retrospective analysis of the Troy mine experience in order to forecast pillar performance at the Montanore mine. The Troy mine and the Montanore mine are less than 30 km apart and is Montana. The Troy mine had a dipping ore body that led to increased shear stresses and a loss in confinement, which resulted in pillar failure. Data was collected on stresses and failure mechanisms and used to calibrate a numerical model to predict pillar performance at the Montanore mine. The result from the study indicated that shear stress was not included when designing the incline pillars at the Troy mine.

Lorig and Cabrera (2013) conducted a numerical study on the effect of foliation and pillar inclination on pillar strength. The model represented width-to-height ratios ranging from 0.3 to 3.5 in intervals of 0.5 and the height of the pillar was fixed at 1.3 m. The geomechanical properties of pillar schist were used to calibrate the model. The results were compared to those of Lunder and Pakalnis (1997) for horizontal pillars. The findings from this numerical study indicated that lower foliation strength would lead to even lower pillar strengths and that steeper inclination also reduces the strength in the pillar.

Discussion

The pillar strength equations available in the literature are site specific and/or does not take into account the shearing effect on inclined seams. Studies have shown that when strength calculations for horizontal pillars are adopted in the case of inclined pillars, they can overestimate the pillar strength and lead to pillar failure mainly due to the fact that horizontal strength equations do not consider the shear stress that acts on an inclined pillar. The three techniques and methodologies identified to estimate inclined pillar strength are analytical solutions, laboratory testing and numerical modeling. The literature review presented in this section demonstrates that numerical modeling can assist with pillar design in inclined orebodies. Furthermore, predictions can be made to improve future mining sustainability when the mining conditions are known, like in the case of Garza-Cruz et al. (2019). In addition, a combination of numerical modeling and laboratory testing can be used to find strength reduction factors, such as conducted by Jessu et al. (2018) and Luo et al. (2020).

2.5 Stability factor

Pillar design depends on pillar strength and pillar stress (Esterhuizen et al., 2008) where strength and stress need to be evaluated for the specific loading mode. The use of stability factors in pillar design typically allows (up to a point) for poor estimations of strength and stress. These principles apply to both coal pillars and non-coal pillars. For stable pillars the pillar strength should always be higher than the stress exerted on the pillar. The stability factor (SF) relates the average pillar strength (S) to the average pillar stress (σ_p) for a flat orebody.

$$SF = \frac{S}{\sigma_p}$$

For coal pillars, it is also well known that pillar strength increases as the pillar width-to-height ratio increases (Mark, 2006) as the core area of the pillar increases. Figure 2.14 schematically presents a typical relationship between pillar strength, pillar stress and the stability factor for different pillar width to height ratios.

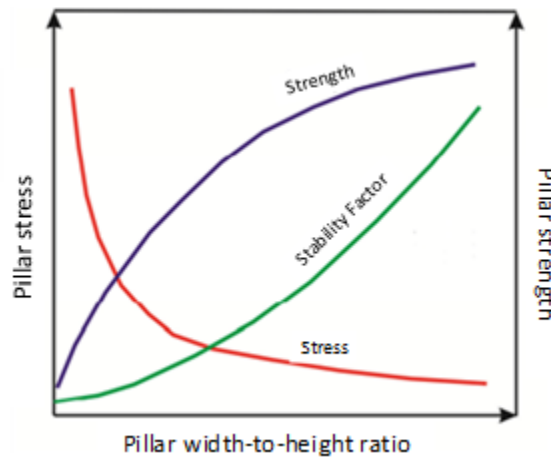


Figure 2.14: The relationship between pillar strength, pillar stress and stability factor (Suorineni, 2013).

According to Merwe et al. (2002), the dip of the seam can affect the pillar stability in coal pillar designs by:

- A reduction in the effective area of the pillar
- The down dip sides of the pillar can spall under the effects of gravity
- The roof strata can ‘ride’ down dip inducing shear at the pillar contact planes
- Non-symmetrical stress distribution may result in higher load on the down dip side.

The approach to estimate the effective pillar dimensions due to inclination, that can be used in pillar strength and stress calculations to estimate the stability factor is shown in Figure 2.15.

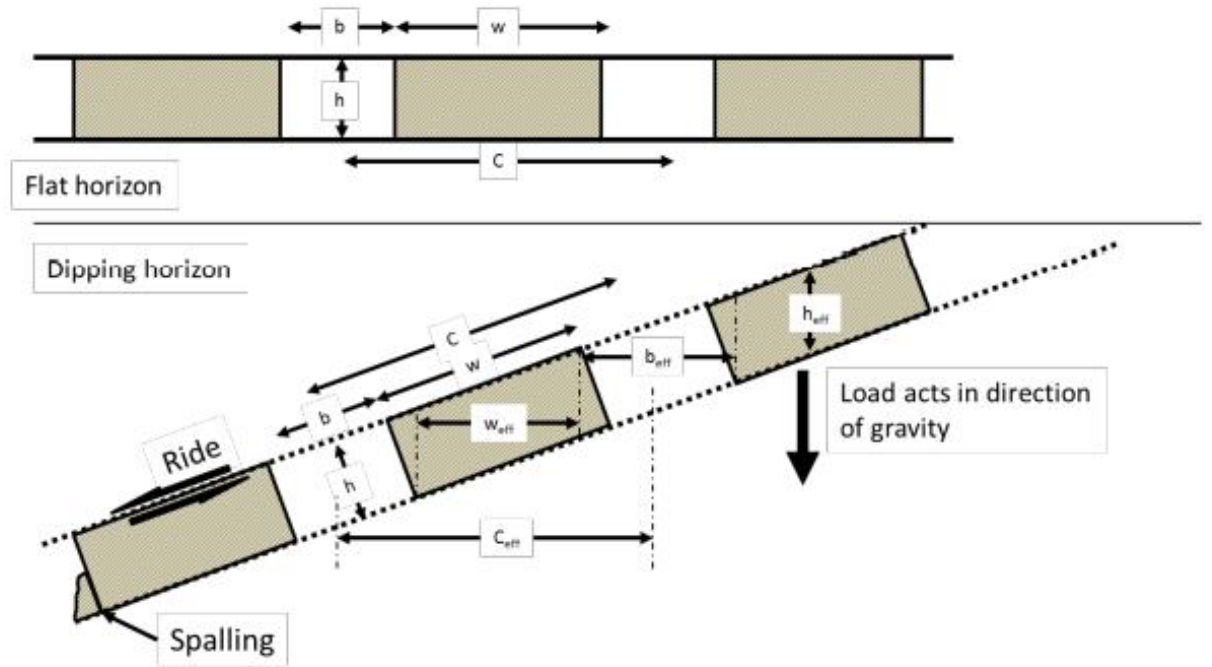


Figure 2.15: Effect of gradient on pillar stability (Merwe et al. 2002).

$$h_{eff} = \frac{h}{\cos\theta}$$

$$w_{eff} = (w - h \tan\theta) \cos\theta$$

$$B_{eff} = (B + h \tan\theta) \cos\theta$$

$$C_{eff} = (b + w) \cos\theta$$

Where:

h_{eff} = Effective pillar height:

w_{eff} = Effective pillar width along the dip:

B_{eff} = Effective board width along dip:

C_{eff} = Effective pillar center distance along dip:

Effective depth, $H_{eff} = H$ at pillar effective mid width ($w_{eff}/2$)

Merwe et al. (2002) also indicated that this approach should only be used for seams that has an inclination of less than 11° , because of the adverse shear effects of steeper inclinations.

Discussion

The stability factor of a pillar is a function of pillar strength and pillar stress. When these parameters are calculated incorrectly due to pillar inclination it can overestimate the stability factor of the pillar which can lead to pillar failure. The analytical approach used by Merwe et al. (2002) is only suitable for seam inclinations less than 11° and indicated that numerical modeling should be used for higher inclinations.

CHAPTER 3. NUMERICAL MODELING

Numerical modeling has proven to be a powerful tool for solving complex geotechnical problems due to its versatility and computational power. Due to the complex loading conditions of inclined orebodies numerous authors have used numerical modeling to investigate how pillar inclination and pillar geometry affect pillar stress. Several researchers (Suorineni (2013), Lorig and Cabrera (2013), Maritz (2015), Jessu and Spearing (2018), Das et al. (2019), Garza-Cruz et al. (2019)) have used numerical modeling to determine pillar stresses and pillar strengths for inclined pillars. A requirement for numerical modeling is the calibration of the models according to known results. The calibration procedure typically consists of evaluation of model results with respect to calculated stress and deformation (and/or other variables) and adjustment of the input parameters in a systematic approach to accomplish a reasonable agreement between the model results and measurements. When models have been calibrated, they can be used to evaluate similar mining designs in similar geological settings (Esterhuizen et al., 2010).

3.1 Model development

Models were created representing a horizontal seam with five pillars with a large width to height ratio such as the pillars present in coal mines. Although this geometry has been modeled extensively by numerous researchers. This step was included as it established a baseline for comparison. Two sets of models were created with respect to inclined pillars. One set features vertical pillar ribs (A-Pillar) and the other features pillar ribs perpendicular to the floor (B-Pillar) (Figure 3.1). Model geometries were developed in RS2, which is a finite element code developed by Rocscience (2022). The pillar and opening dimension in these models are hypothetical, however their inclination and pillar geometry are based on information available in the literature as discussed above.

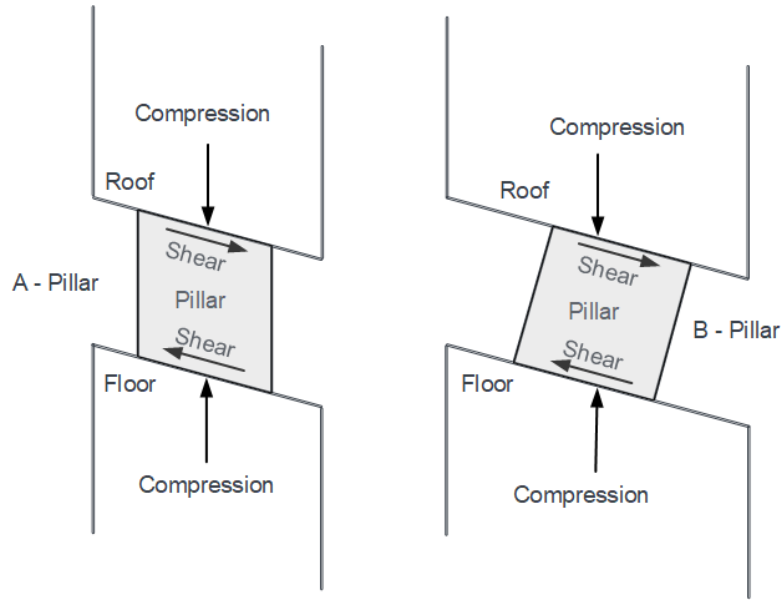


Figure 3.1: Geometry of models developed.

Inclined pillar models included five (5) pillars for various inclinations and two rib geometries, shown in Figure 3.2 and Figure 3.3. The inclined-pillar geometry was modeled using five (5) pillars instead of a single inclined pillar as the latter does not actually model the behavior of a series of pillars on an inclined seam (Lorig and Cabrera, 2013). Stresses were extracted for the middle pillar. The models assumed competent roof and floor (sandstone) and typical coal properties for the pillar. The initial runs were under an elasticity assumption for all materials. It is understood that a 2D plane strain model refers to a very long pillar in the out-of-plane direction, however, the objective of this study is to compare the stresses developed across the different geometries.

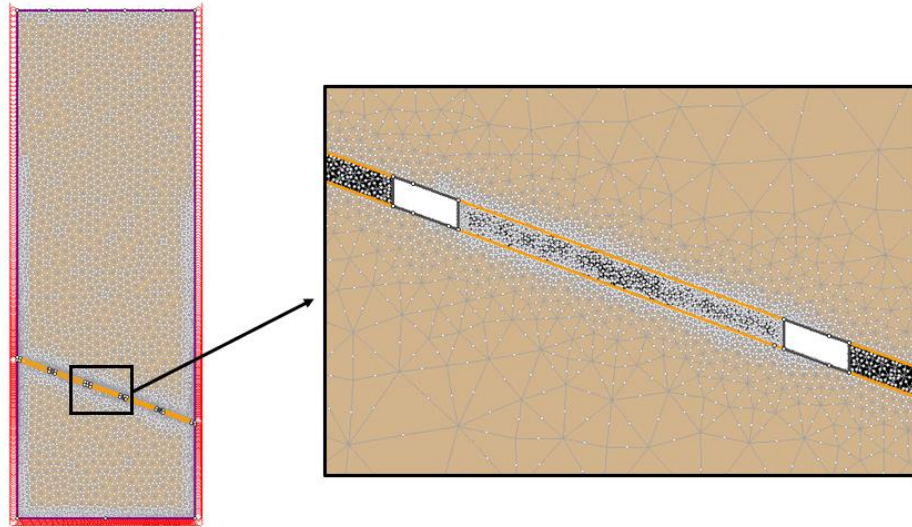


Figure 3.2: Model of a 20° inclined pillar with vertical pillar ribs (A-Pillar).

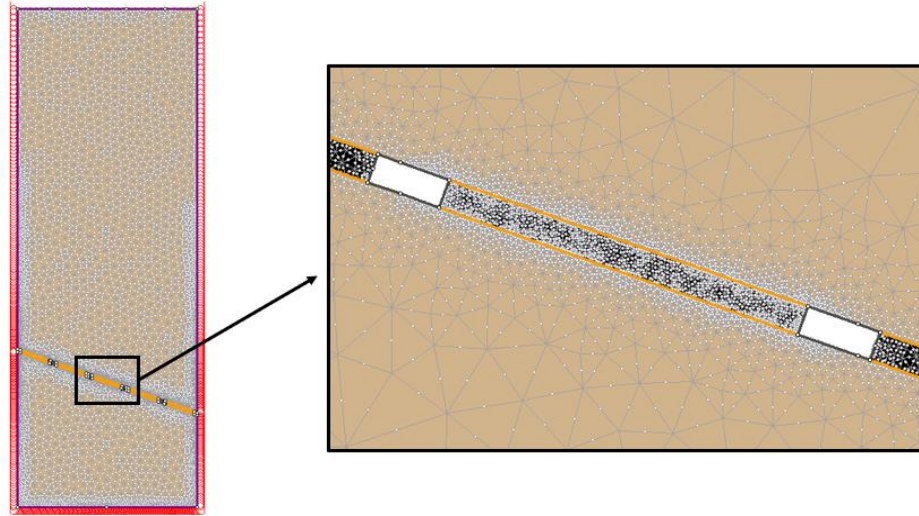


Figure 3.3: Model of a 20° inclined pillar with pillar ribs perpendicular to the floor (B-Pillar).

The material properties that were used for sandstone and coal for the elastic models in this study was gathered from work done by Tulu et al. (2017) and Esterhuizen et al. (2010). The material properties for coal and sandstone are shown in Table 3.1 and Table 3.2 respectively.

Table 3.1: Elastic parameters of sandstone (Tulu et al., 2017)

Parameter	Value
Unit weight (MN/m ³)	0.024
Young's modulus (MPa)	20460
Poisson's ratio	0.25

Table 3.2: Elastic parameters of coal (Esterhuizen et al., 2010)

Parameter	Value
Unit weight (MN/m ³)	0.0196
Young's modulus (MPa)	3000
Poisson's ratio	0.25

Subsequently failure criteria were introduced for both the coal and the roof and floor rock which was modelled as a much stronger material (sandstone). The lab UCS strength of the pillar material (coal) was modelled with varying strength values. The sandstone properties remained the same as in the elastic model. Coal was modelled as an elastoplastic material using the strain-softening option. The material properties that were used for the constitutive models were gathered from Esterhuizen et al. (2010) and are shown in Table 3.3. The strain softening option allows the material to assume residual stresses in the highly stressed regions (i.e., ribs) which push the peak stresses towards the core of the pillar.

Table 3.3: Material properties for Hoek-Brown Constitutive Model (Esterhuizen et al.,2010).

Parameter	Value
Unit weight (MN/m ³)	0.0196
Young's modulus (MPa)	3000
Poisson's ratio	0.25
UCS (MPa)	10, 15, 20
m-value	1.47
s-value	0.07
m-Residual	1
s-Residual	0.001

An interface element was added between the coal and the sandstone to allow for relative slippage, i.e., between the roof and the pillar as the pillar deforms (Figure 3.4).

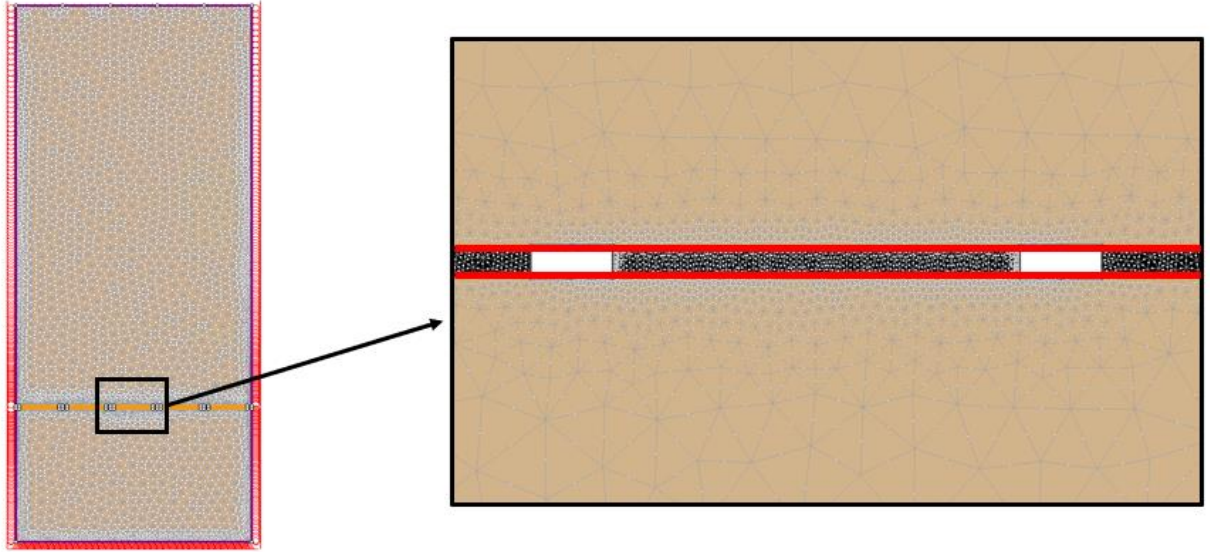


Figure 3.4: Shows the interface elements that was added between the sandstone and the coal.

The material properties for this interface elements was gathered from work done by Esterhuizen et al., (2010) and is shown in Figure 3.4.

Table 3.4: Material properties for the interface element (Esterhuizen et al., 2010).

Parameter	Value
Interface normal stiffness (GPa/m)	100
Interface shear stiffness (GPa/m)	50

3.2 Numerical Analysis

Five (5) rectangular pillars with a width of 25 m and a height of 2 m were modeled in a horizontal geometry (Figure 3.5) as well as in 10-, 20-, and 30-degree inclinations. The inclined pillars were modeled both as A-Pillars and as B-Pillars (Figure 3.2 and Figure 3.3). The overburden depth was set to 300 m with an overburden specific weight of 24 kN/m³. In-situ horizontal stresses were set to one third of the vertical stress. The tributary area stress for a very long horizontal pillar with the same width was calculated at 8.64 MPa. This is considered a reference value for the average stress across a pillar as calculated by the 2D plane strain finite element models.

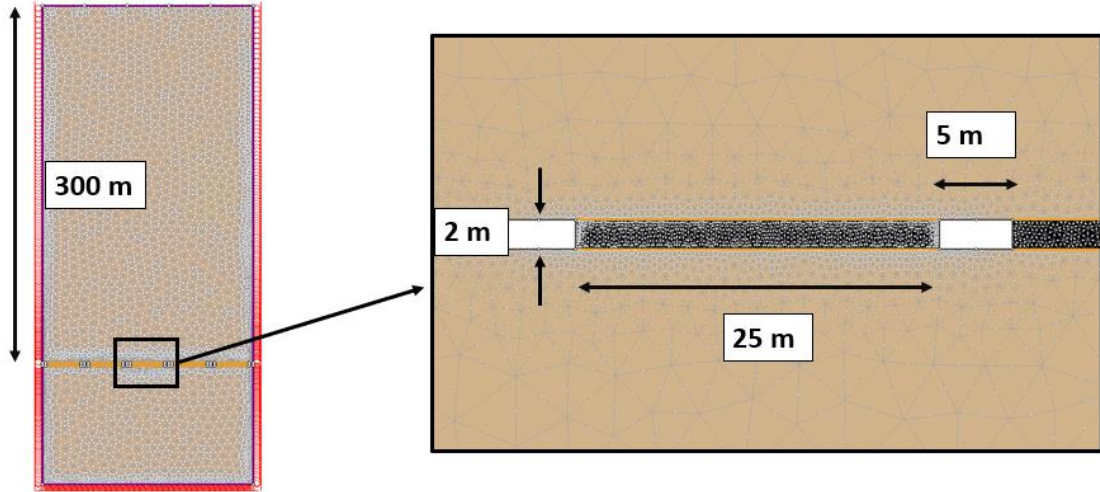


Figure 3.5: Model of the Horizontal pillar dimensions.

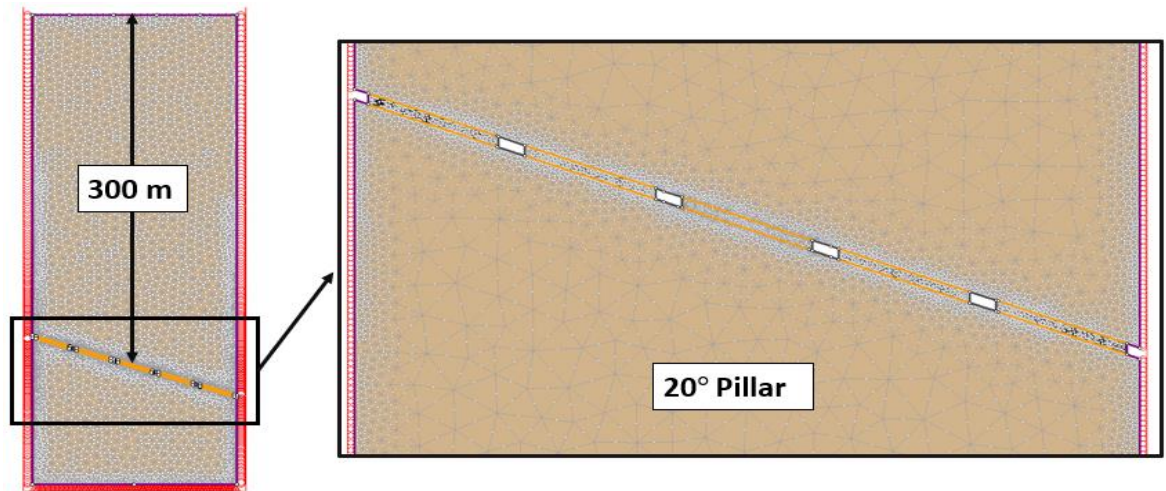


Figure 3.6: Model of five 20° Inclined A-pillars.

Before finalizing the models, a sensitivity analysis was developed with respect to mesh size. The analysis determined the size of the mesh required for both the pillar and the surrounding rock to ensure reliable calculations for stresses and strains. A mesh gradation factor of 0.1 (default value) was used that resulted in a fine mesh around the entry and larger elements away from the entry. Figure 3.7 compares mesh that were developed with gradation factors 0.1 and 0.01.

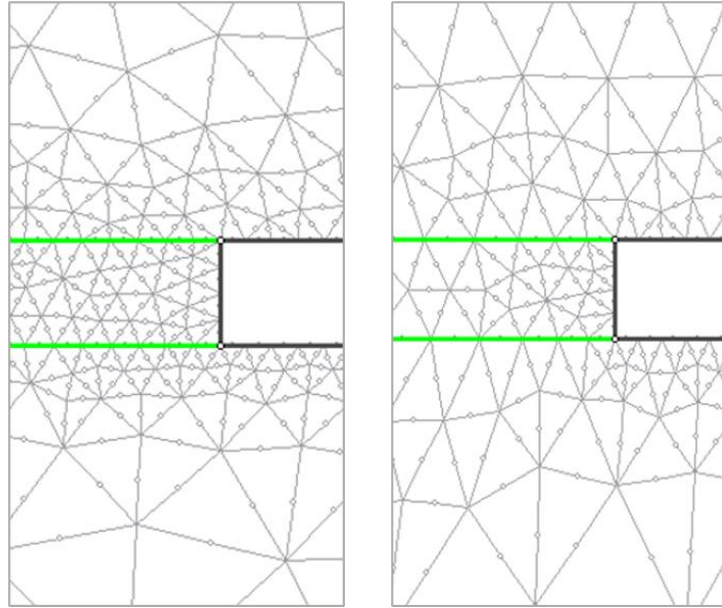


Figure 3.7: Left: Mesh with a gradation factor of 0.1. Right: Mesh with a gradation factor of 0.01.

An increased mesh discretization density was added to the center pillar where the stress measurements were taken Figure 3.8. This was done to ensure more accurate results.

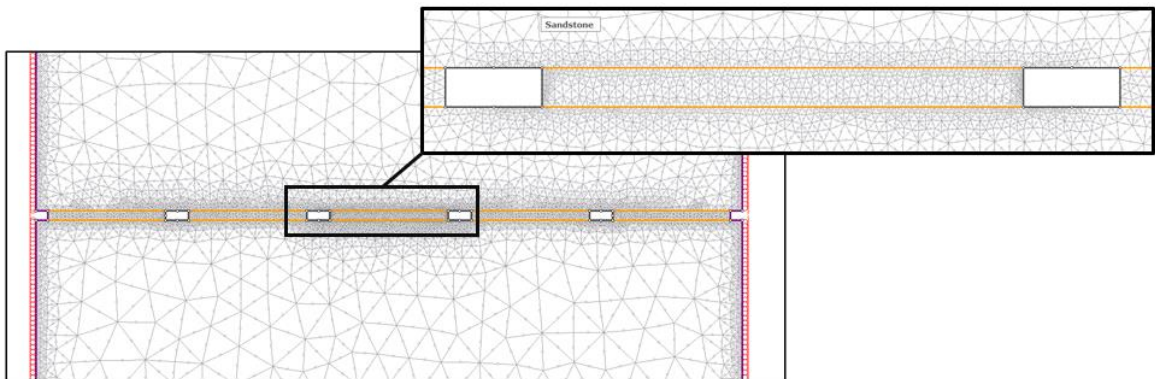


Figure 3.8: Increased mesh discretization density around the center pillar.

The elastoplastic models were run with three different values with respect to the material lab strength. Figure 3.9 and Figure 3.10 show the models that were developed for elastic material properties and for elastoplastic pillar properties for both the cases of the A-pillar and the B-pillar. Seven elastic and 28 Hoek & Brown models were generated. All models utilized a six-node triangular element and a graded mesh with about 19 000 nodes and 9000 elements.

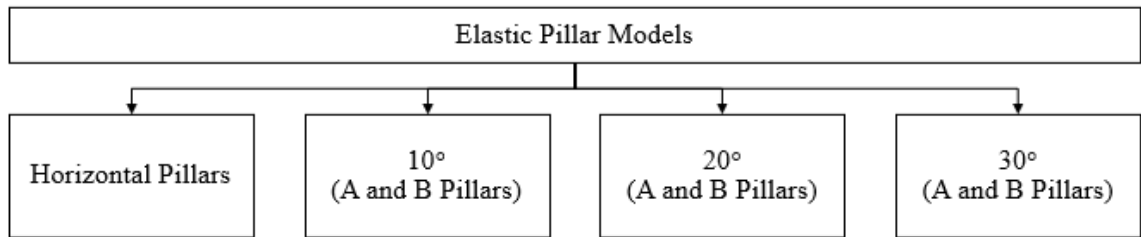


Figure 3.9: Model geometries for elastic models.

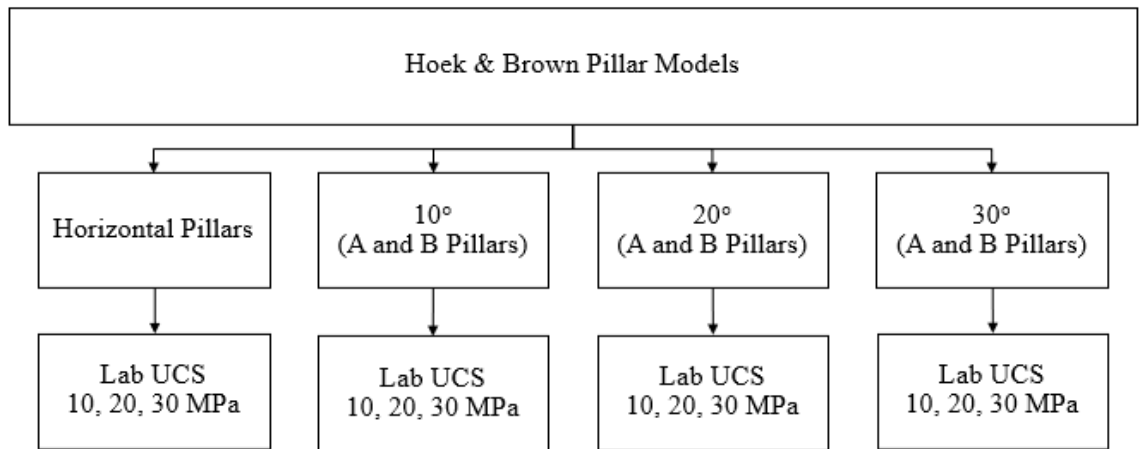


Figure 3.10: Model geometries for Hoek & Brown models.

CHAPTER 4. RESULTS AND DISCUSSION

In this study a total of 35 numerical models were developed, based on the same pillar dimensions with variations in the seam inclination (0° , 10° , 20° and 30°), the orientation of the pillar ribs and the UCS values of the coal. This section discusses the influence of these parameters on the major principal stress as well as the shear stresses. The stresses were numerically calculated along the pillar width at mid height and along the pillar-roof interface. Elastic models were used to compare the impact on the development of such stresses due to elastic behavior and pillar geometry. Additionally, Hoek & Brown models were also generated to investigate the effect of different coal UCS values and seam inclination has on the developed stresses.

4.1 Major principal stress

The major principal stress results were taken along the center pillar width at mid height, shown in Figure 4.1.

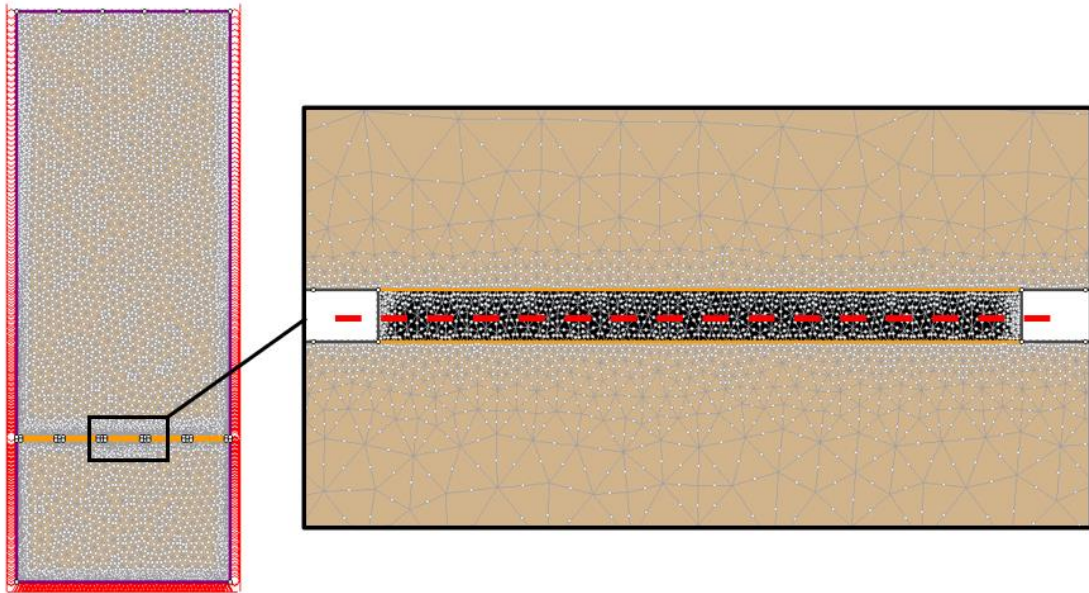


Figure 4.1: Location of the major principal stress queries.

4.1.1 Major principal stress under elastic conditions

Figure 4.2 presents the variation of major principal stress along the pillar width at mid height for an elastic regime for four different seam inclination angles and different pillar geometries. The major principal stresses peaks close to the rib and it decreases towards the center of the pillar. Right at the rib there is a reduction in stress with respect to the peak which is a result of rib deformation due to the specific opening geometry. This is different

than distributions observed for other opening geometries (i.e., circular) where peak principal stresses occur right at the rib (Obert & Duvall, 1967). In addition, the major principal stress increases slightly as seam inclination increases.

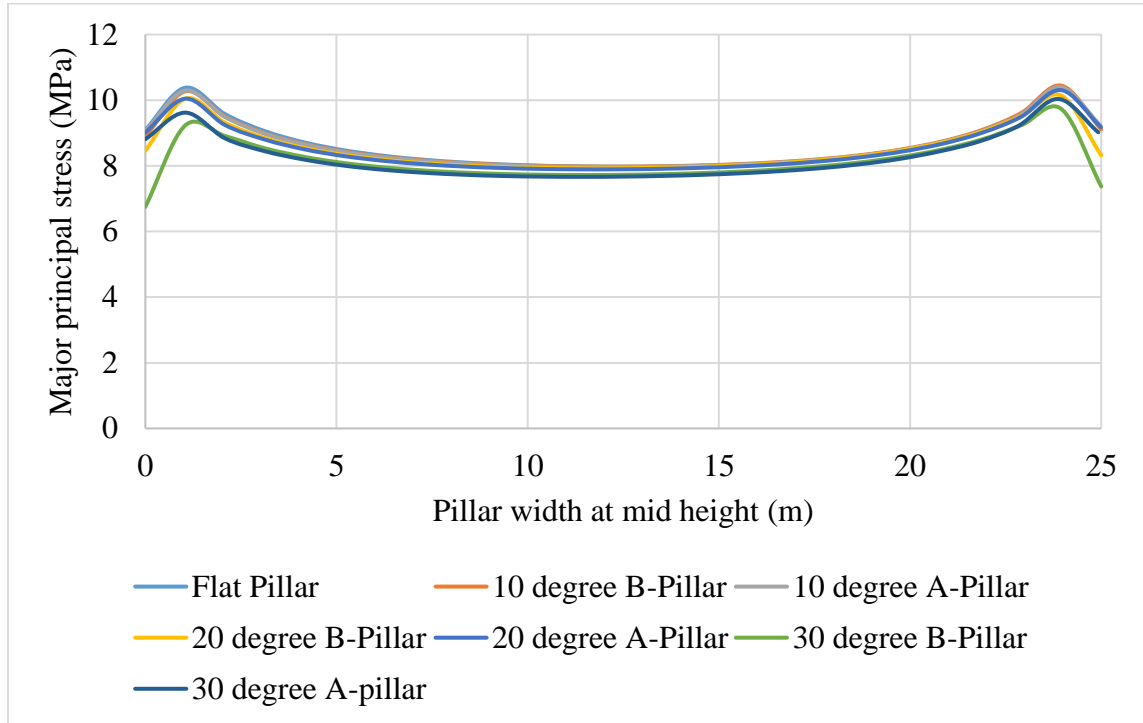


Figure 4.2: Elastic major principal stress results.

Figure 4.3 compares the elastic major principal stress results for a 30° inclined A- and B-Pillar. Close to the rib region the variation between the different geometries is more pronounced and lower rib stresses are experienced in the case of the perpendicular pillar geometry (B-Pillar). The main body of the pillar is almost the same as expected.

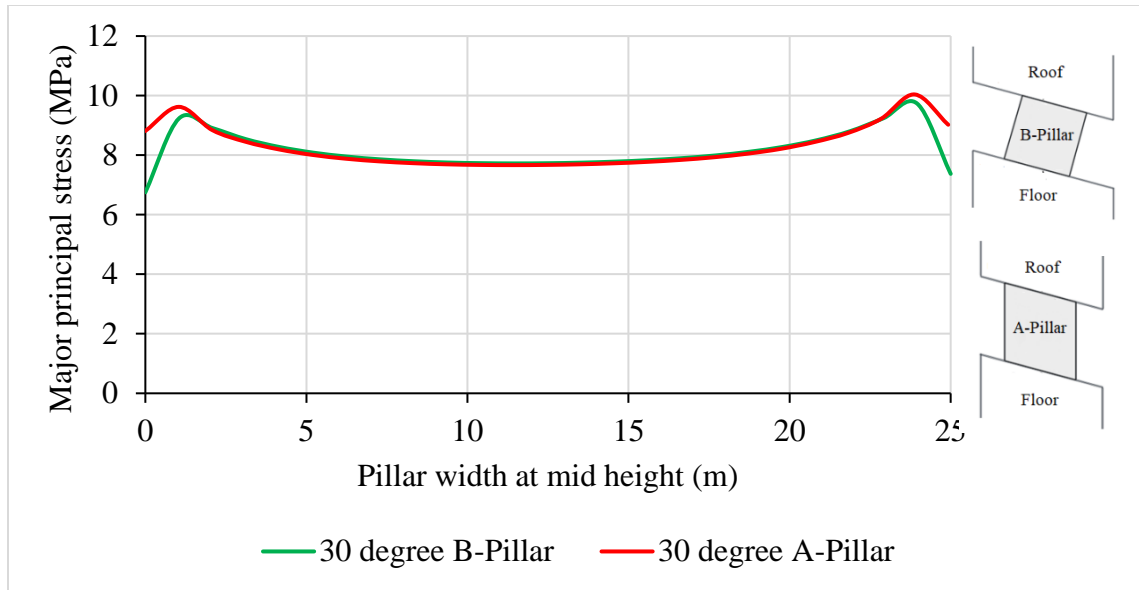


Figure 4.3: Elastic major principal stress results for a 30° inclined A- and B-Pillar.

Figure 4.4 and Figure 4.5 illustrate the orientation of the major principal stress for a flat and 30° inclined A-Pillar. In both cases the direction of the major principal stress in the vicinity of the pillar follows the direction of loading.

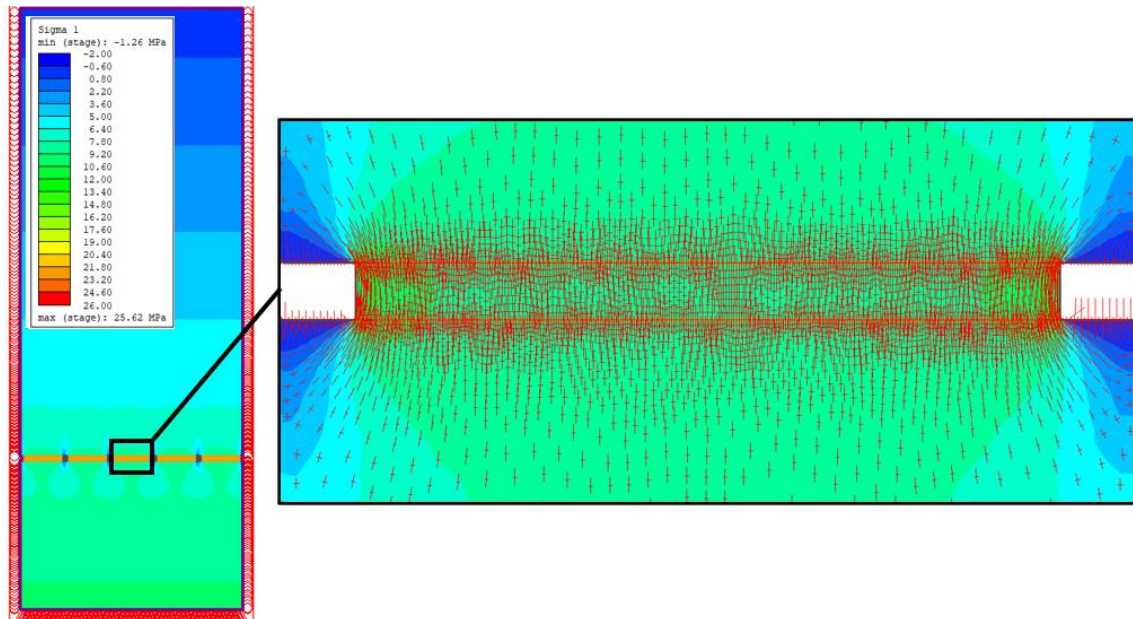


Figure 4.4: Orientation of the major principal stress for an elastic flat pillar.

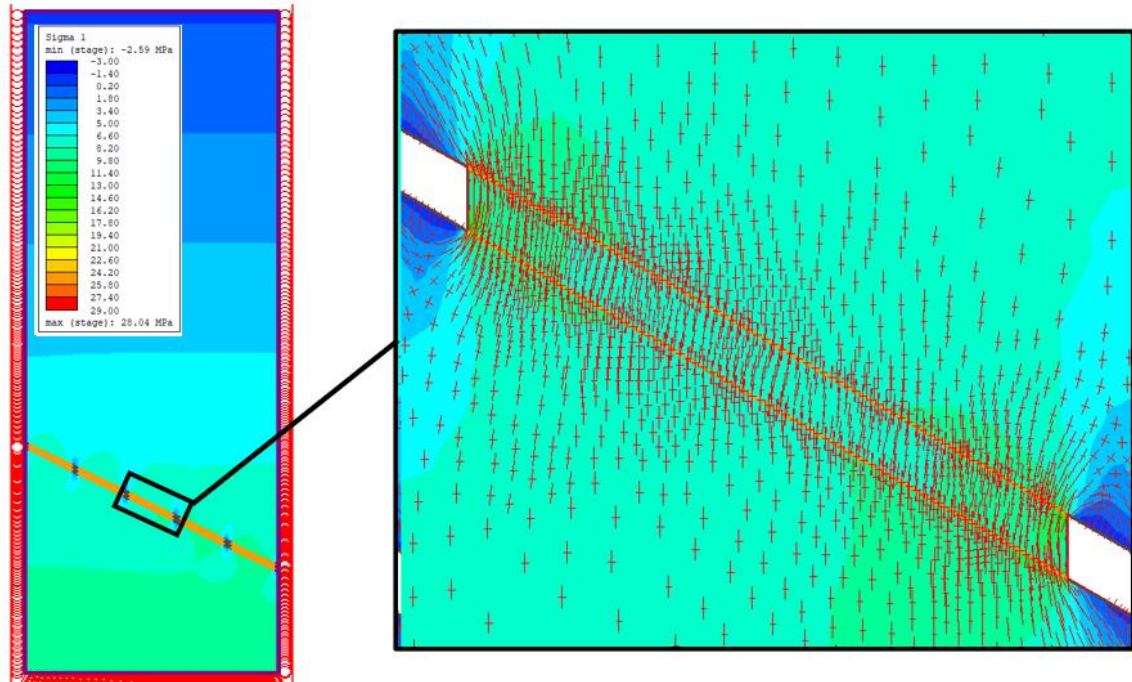


Figure 4.5: Orientation of the major principal stress for an elastic 30° inclined A-Pillar.

Figure 4.6 and Figure 4.7 illustrate the total displacement vectors for a flat and a 30° inclined A-Pillar. As expected, the overburden weight will cause a reduction in opening size. Both models are under elastic conditions, and the rib material has not failed. In both cases the total displacement vectors follow the direction of loading.

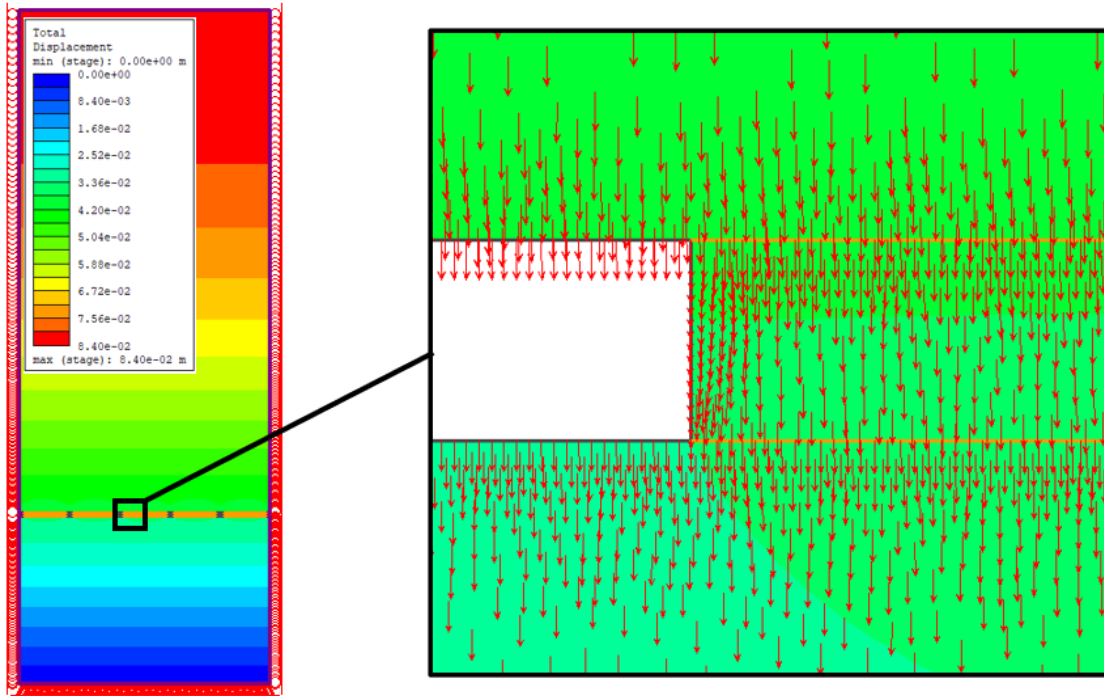


Figure 4.6: Displacement vectors for an elastic flat pillar.

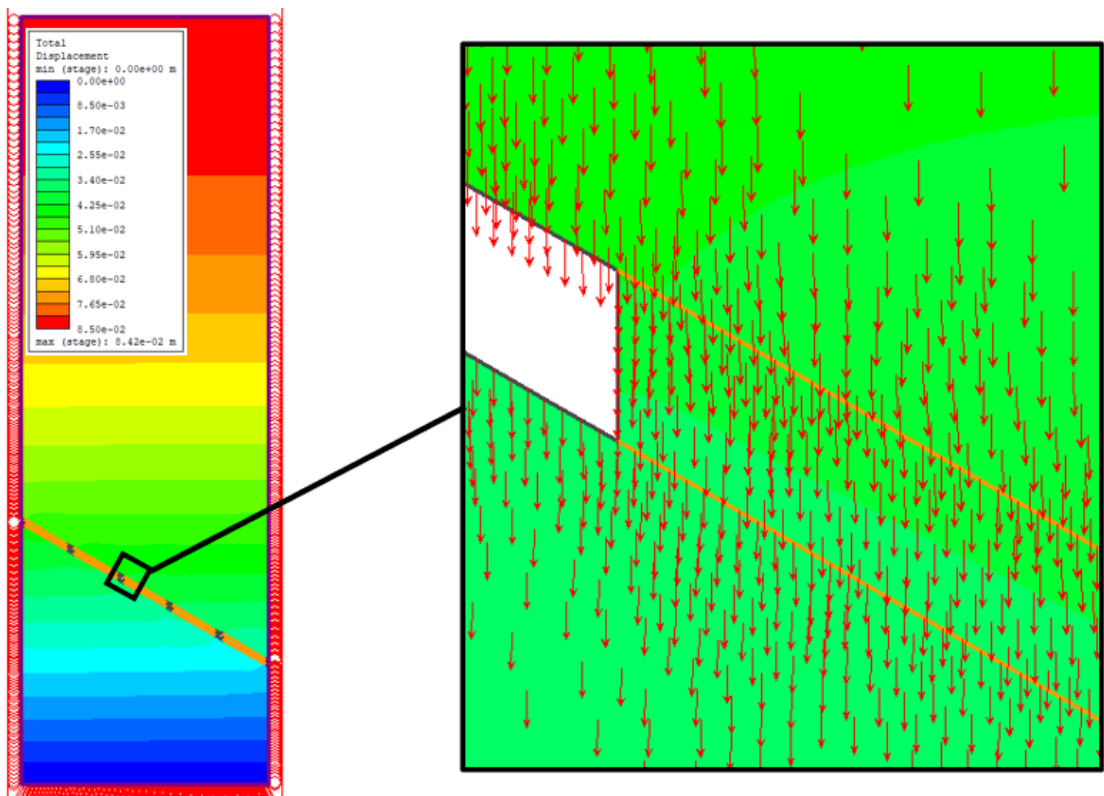


Figure 4.7: Displacement vectors for an elastic 30° inclined A-Pillar.

4.1.2 Major principal stress under the Hoek & Brown criterion

The variation of the major principal stress for the same line query, for a Hoek & Brown strain softening regime is presented in the case of the horizontal pillar (Figure 4.8) and the 20° inclined A-pillar (Figure 4.9). Zero values are denoted at the ribs, in contrast to the non-zero values in Figure 4.2 (elastic case). The effect of different coal UCS values were also investigated, for both horizontal and inclined pillars. For the UCS values selected the peak values of the major principal stress on the pillar are not really affected. As expected, the peak stress value appears further away from the ribs as the UCS value decreases, which confirms that the yielded region (that develops at the rib towards the center of the pillar) increases as the coal UCS decreases.

As expected in Figure 4.8 and Figure 4.9, stresses are high at the center (core) of the pillar, while they quickly dissipate away from the center of the pillar and close to the rib. The actual peak is not at the center of the pillar but at the transition between the yielded zone and the core. This is attributed to the fact that the rib has yielded due to high stress conditions and therefore the rib material can only bear very low or even zero loads. This is the same behavior observed in horizontal pillars modelled under elastoplastic conditions (Cardenas Triana et al., 2021).

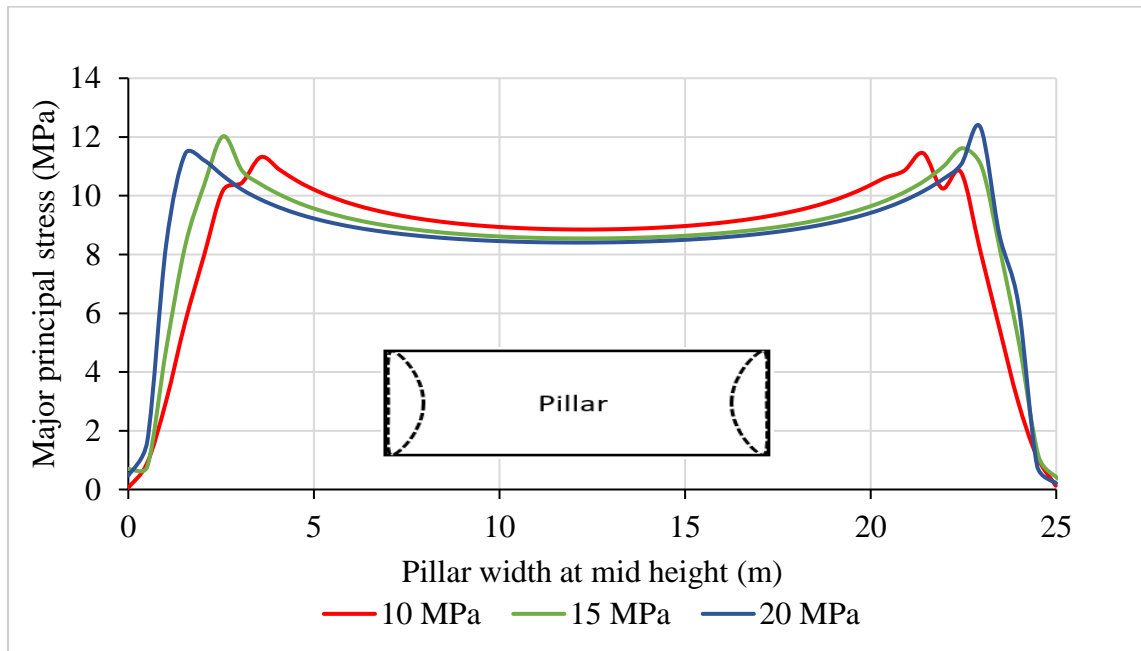


Figure 4.8: Variation of the major principal stress along the pillar width at mid height for the Hoek & Brown models for different coal UCS values for the horizontal pillar.

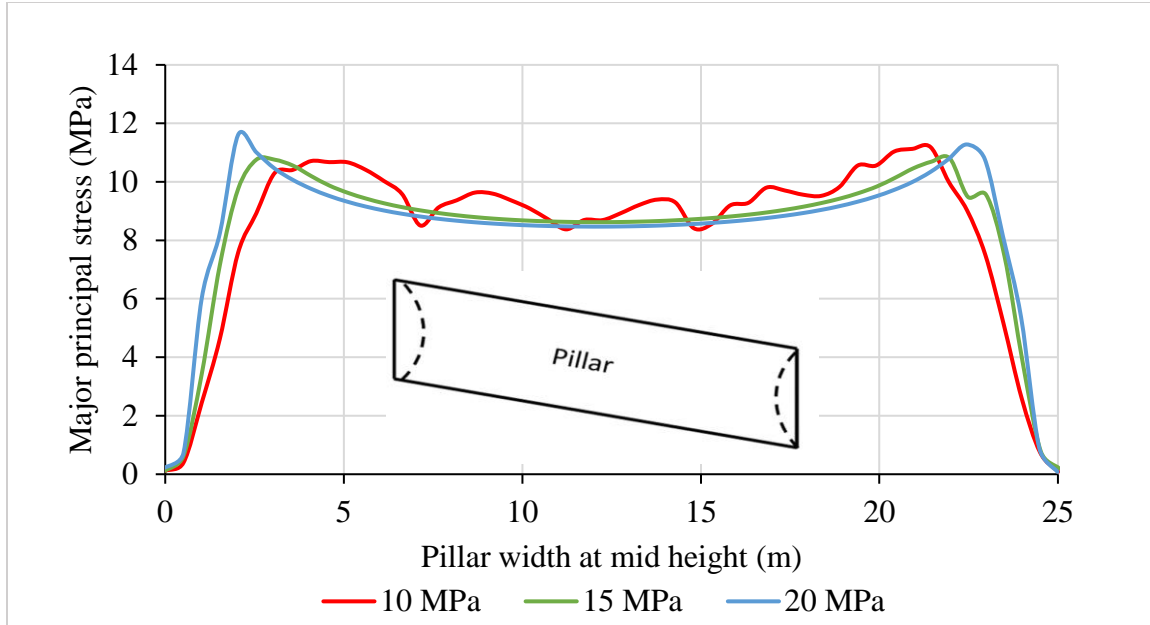


Figure 4.9: Variation of the major principal stress along the pillar width at mid height for the Hoek & Brown models for different coal UCS values for the 20° inclined A- Pillar.

Figure 4.10 compares the major principal stress for different seam inclinations with vertical pillar rib geometries (A-Pillar) and for a coal UCS value of 20 MPa. In the core of the pillar the stresses are the same and it increases as you get closer to the ribs. The stresses do not peak at the rib but peaks a few meters into the pillar. The stresses at the rib are zero which indicates that the rib material has yielded. This is similar to the findings presented in the paper written by Jessu et al., (2018). The peak stress decreases as the seam inclination increases.

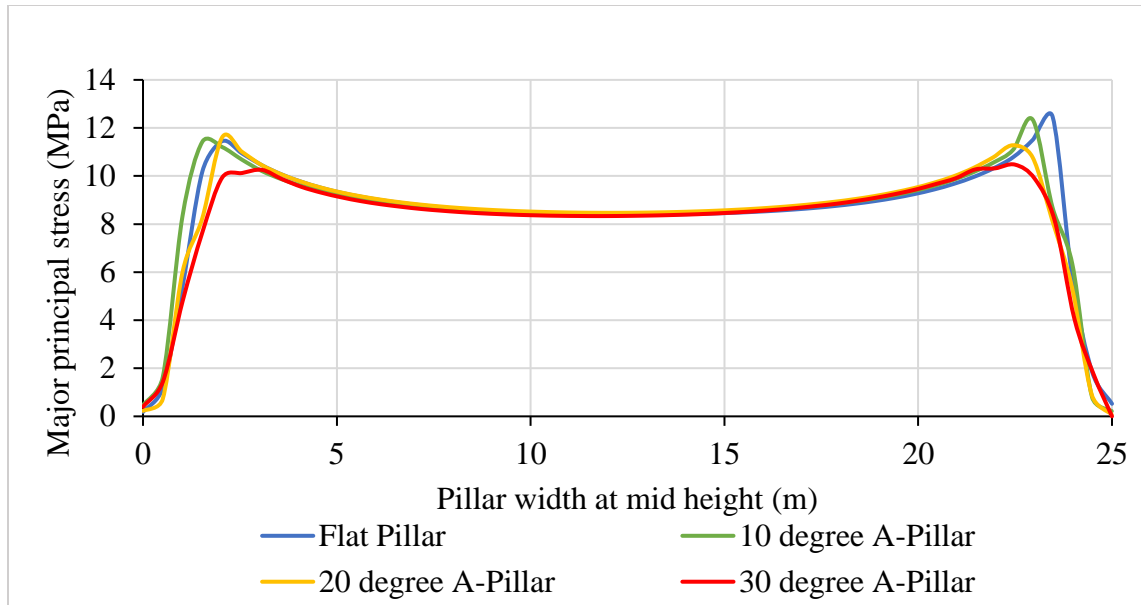


Figure 4.10: Comparison of the major principal stress and different inclination with a vertical pillar geometry (A-Pillar), with a coal UCS of 20 MPa.

Figure 4.11 compares the major principal stress for a vertical and perpendicular (A – and B-Pillar) pillar geometry. The stress in the two geometries is the same and there is no distinct difference.

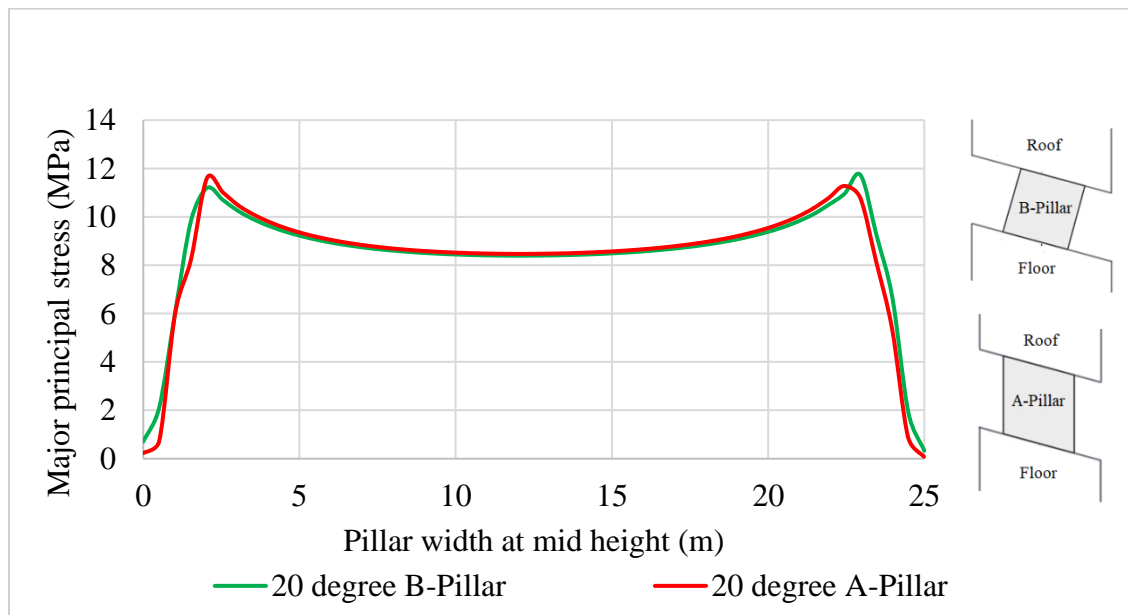


Figure 4.11: Variation of the major principal stress along the pillar width at mid height for the Hoek & Brown models in the case of the 20° inclined A- and B-Pillar, with a coal UCS of 20 MPa.

Figure 4.12 and Figure 4.13 shows the direction of the major principal stress for a flat and 20° A-Pillar under Hoek & Brown conditions.

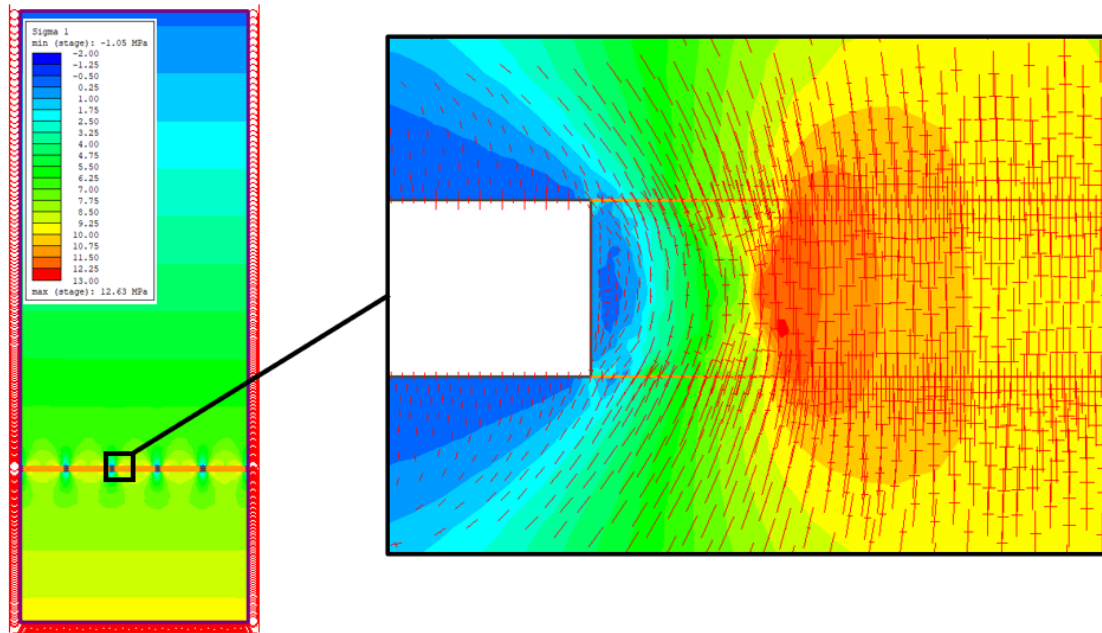


Figure 4.12: Orientation of the major principal stress for a 15 MPa Hoek & Brown flat pillar.

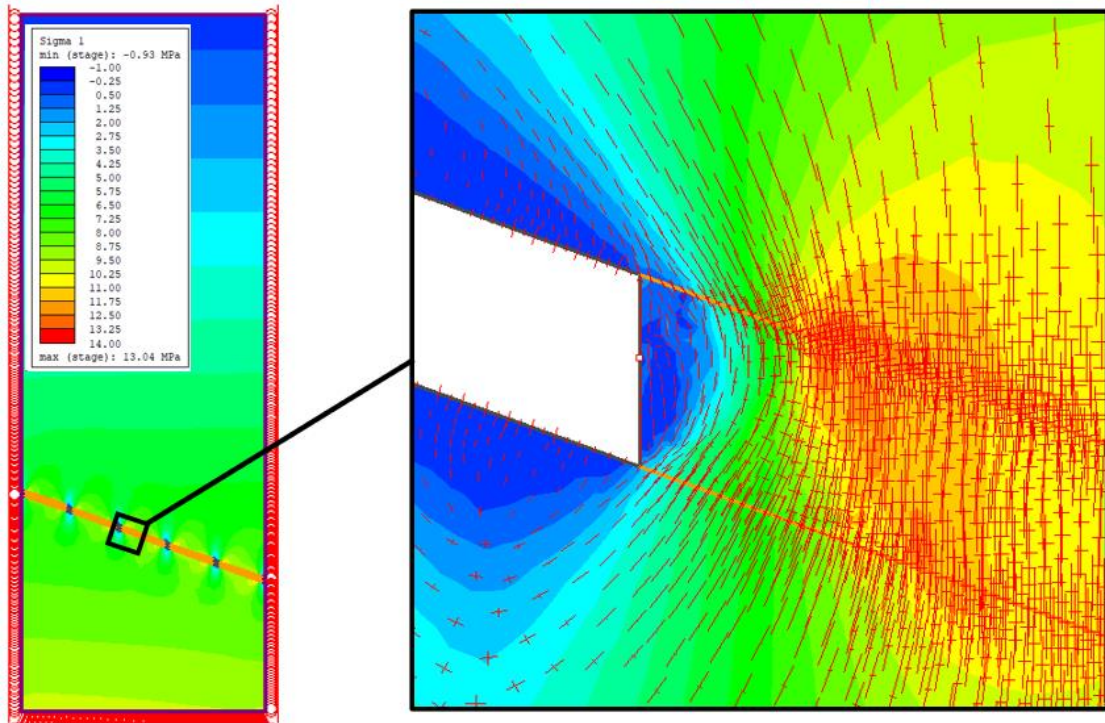


Figure 4.13: Orientation of the major principal stress for a 15 MPa Hoek & Brown 20° A-Pillar.

Figure 4.14 and Figure 4.15 shows the displacement vectors for a flat and 20° A-Pillar under Hoek & Brown conditions. In contrast with the elastic models the rib material is starting to yield. This is illustrated by the displacement vectors at the rib pointing in a down-outwards direction.

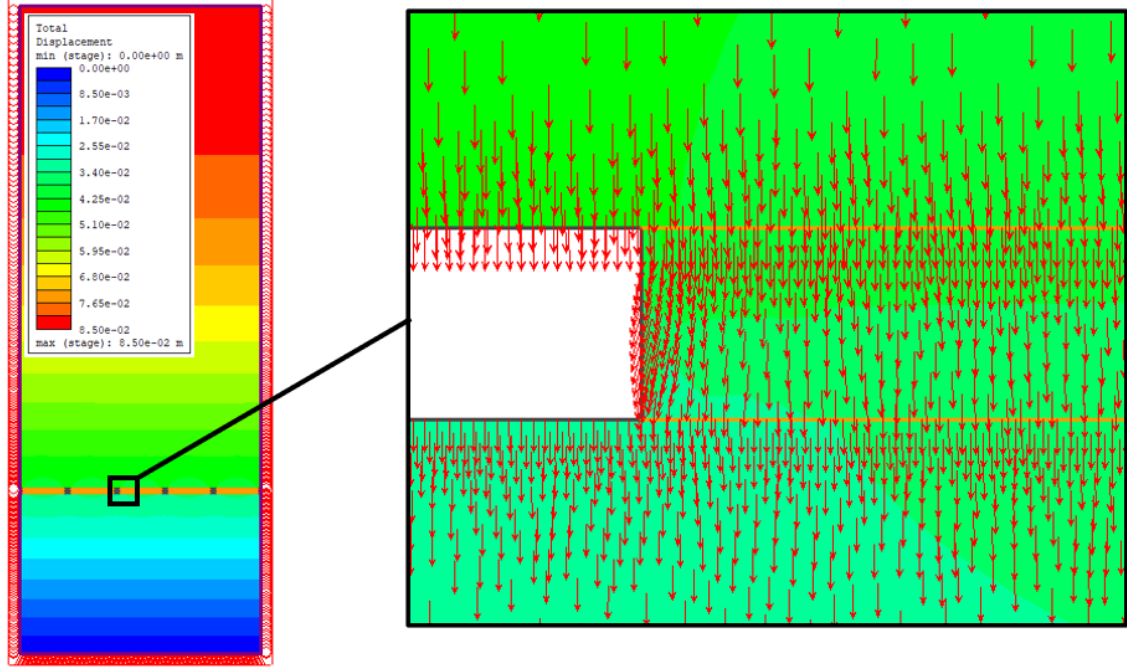


Figure 4.14: Displacement vectors for a 15 MPa Hoek & Brown flat pillar.

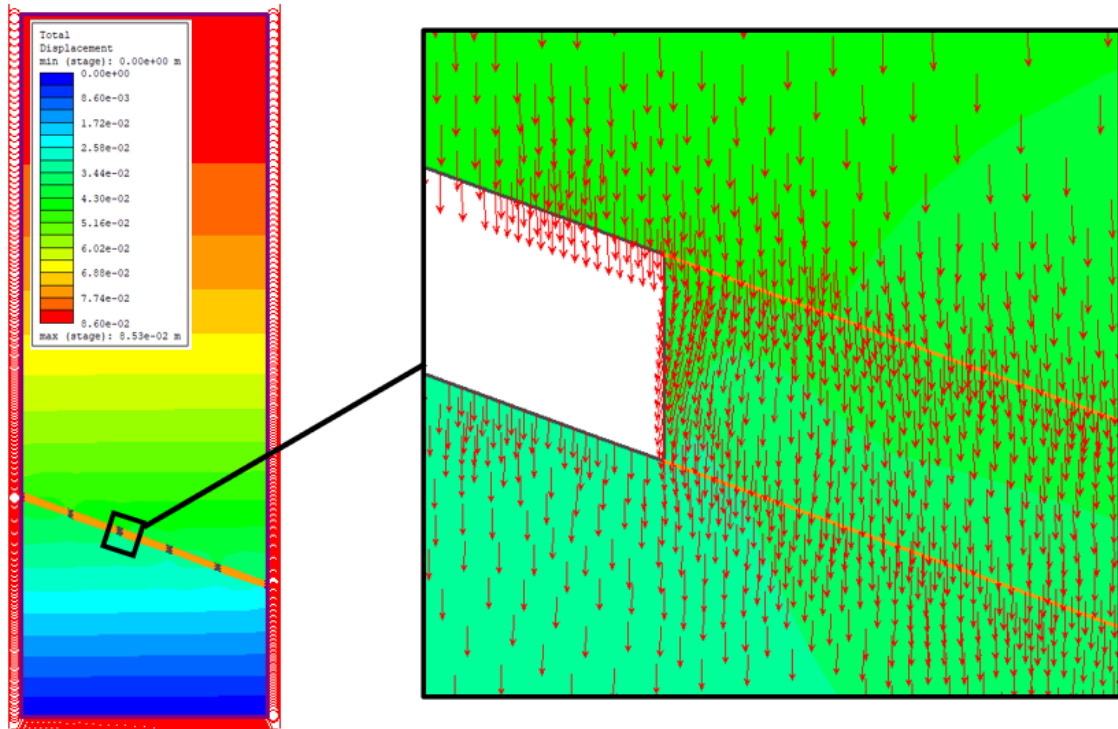


Figure 4.15: Displacement vectors for a 15 MPa Hoek & Brown 20° A-Pillar.

4.1.3 Comparison between the elastic and Hoek & Brown models

Figure 4.16 compares the major principal stress between the elastic and Hoek & Brown models for a flat pillar and 20° inclined A-Pillar. At the rib region, the elastic models experience higher stresses than the Hoek & Brown models. This is due to fact that the rib material has failed in the Hoek & Brown models and, therefore, it can bear much lower loads. The major principal stresses in the Hoek & Brown models are translated more towards the core of the pillar which leads to higher peak stresses than the elastic models.

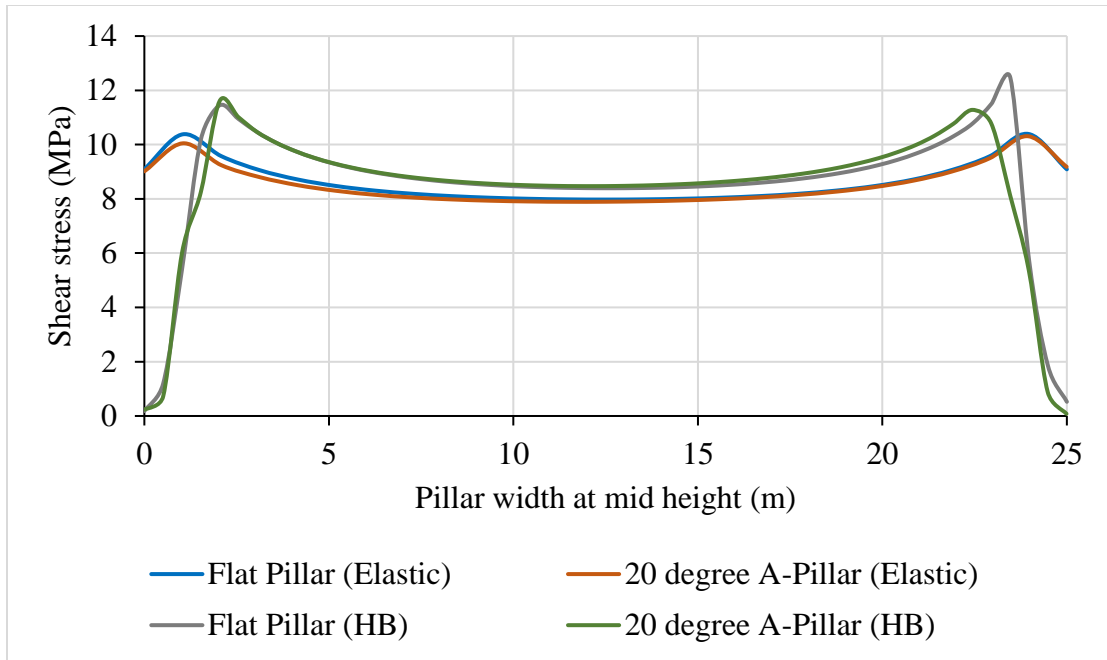


Figure 4.16: Comparison of the major principal stress between the elastic and Hoek & Brown models for a flat pillar and 20° inclined A-Pillar.

4.2 Shear stress at the pillar-roof interface

The shear stress results were taken along the center pillar width, at the pillar-roof interface, shown in Figure 4.17.

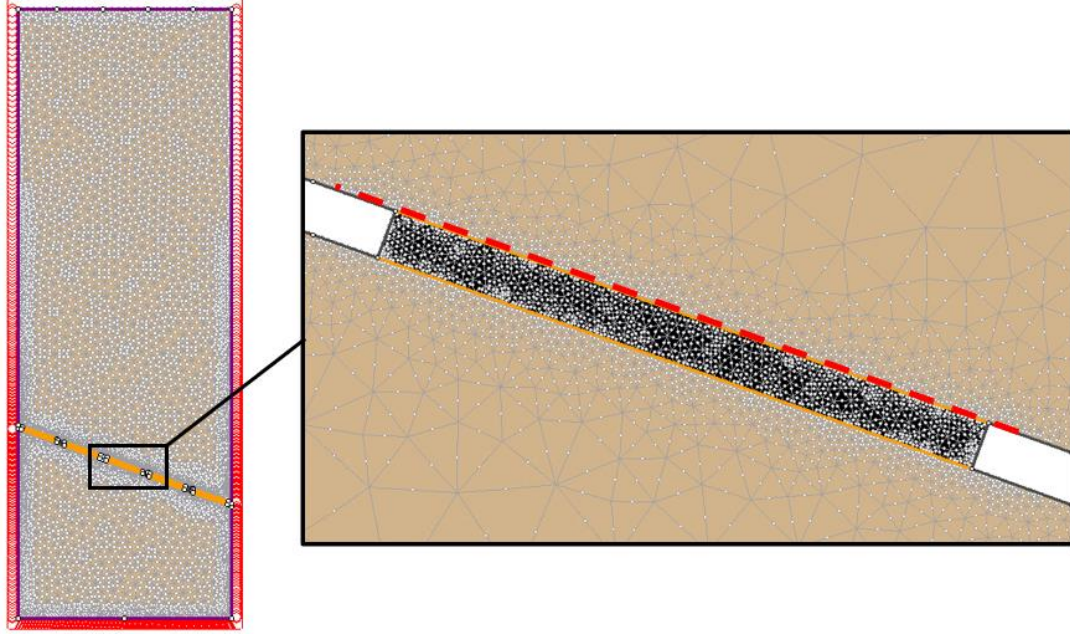


Figure 4.17: Location of the shear stress queries.

To calculate the shear stress on a plane the following equation was used. The stress element, Figure 4.18, can be used to better understand this equation.

$$\tau_n = -\frac{1}{2}(\sigma_x - \sigma_y) \sin 2\theta + \tau_{xy} \cos 2\theta$$

Where,

σ_x = Stress in the x -direction

σ_y = Stress in the y -direction

τ_{xy} = Shear stress

θ = Angle between the x -axis and the normal to the plane under study (same as the stress σ_n direction)

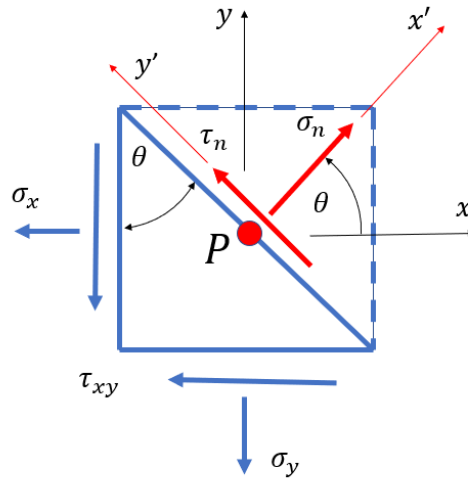


Figure 4.18: Stress element.

4.2.1 Rotated shear stress at the pillar-roof interface under elastic conditions

Figure 4.19 compares the distribution of the shear stress along the pillar-roof interface for different pillar inclinations with vertical and perpendicular (A- and B-Pillar) geometries. A rapid change of shear stress is observed close to the rib regions. On the uphill side the change of shear stress is positive while on the downhill side the change of shear stress is negative. The reason for this is that there is a change in direction of the shear stress at the pillar ribs between the uphill and downhill side. The peak shear stresses are higher on the uphill side of the pillar than the downhill side. As expected, when the seam inclination increases the shear stress also increases.

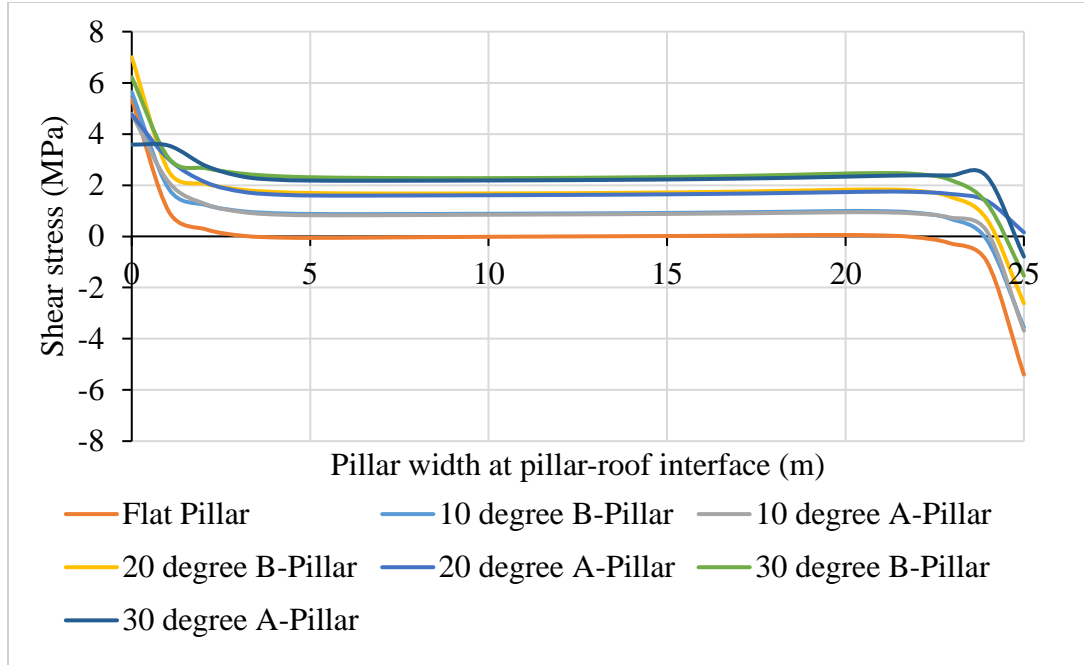


Figure 4.19: Variation of the shear stress along the pillar-roof interface with respect to the seam inclination in elastic models.

The maximum shear stress values at the ribs for the perpendicular pillar (B-pillar) are slightly higher than those of the vertical pillar (A-pillar) on the uphill side, shown in Figure 4.20. This may be attributed to the inclination of the pillar with respect to the roof and floor lines.

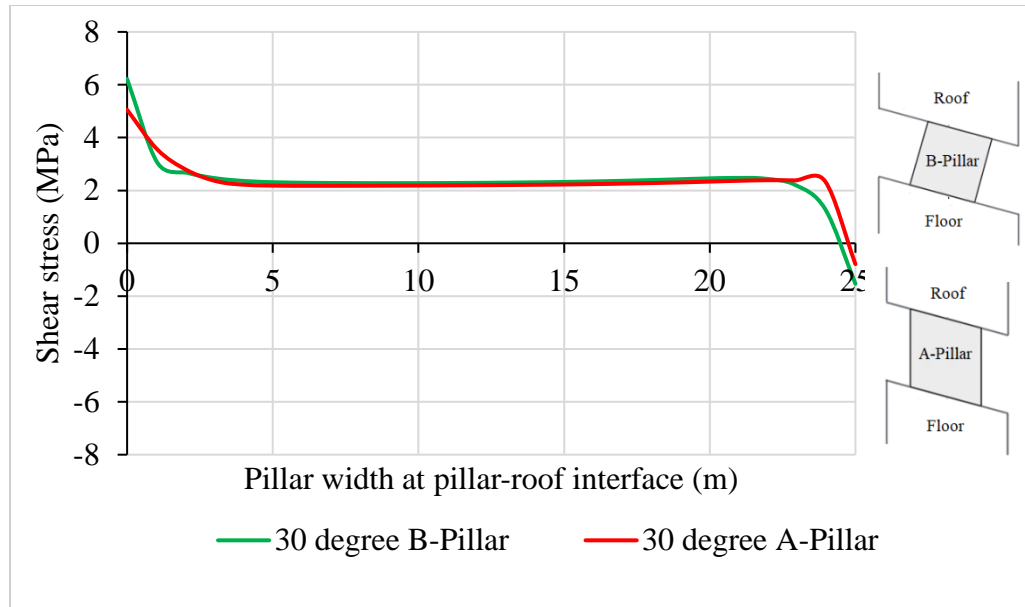


Figure 4.20: Variation of the shear stress along the pillar-roof interface for elastic models in the case of the 30° inclined A- and B-Pillar.

4.2.2 Rotated shear stress at the pillar roof interface using the Hoek & Brown criterion

Figure 4.21 compares the shear stress at the pillar roof interface for different inclinations and pillar geometries with a coal UCS of 20 MPa. The peak shear stresses are lower in Hoek & Brown models when compared to elastic models (Figure 4.19). In contrast with the elastic models the peak shear stresses are not at the rib, but a few meters into the rib. This is due to the rib material that has yielded. This means that the pillar can take lower to zero loads. When the seam inclination increases the shear stress at the pillar-roof interface also increases, as expected.

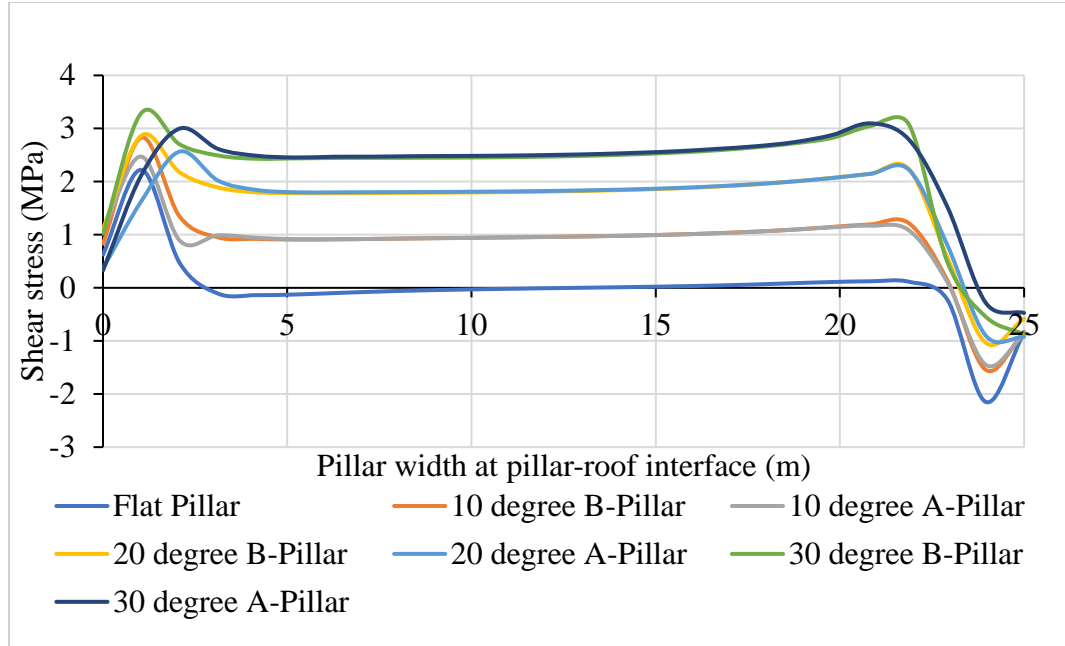


Figure 4.21: Variation of the shear stress along the pillar-roof interface with respect to the pillar inclination for Hoek & Brown models with coal UCS = 20 MPa.

Figure 4.22 compares the shear stress at the pillar roof interface for different inclinations and pillar geometries with a coal UCS of 10 MPa. It is observed that a low coal UCS values and high pillar inclinations the Hoek & Brown models struggle to converge and is presented by oscillating lines. This is due to the numerical solution of the strain softening model.

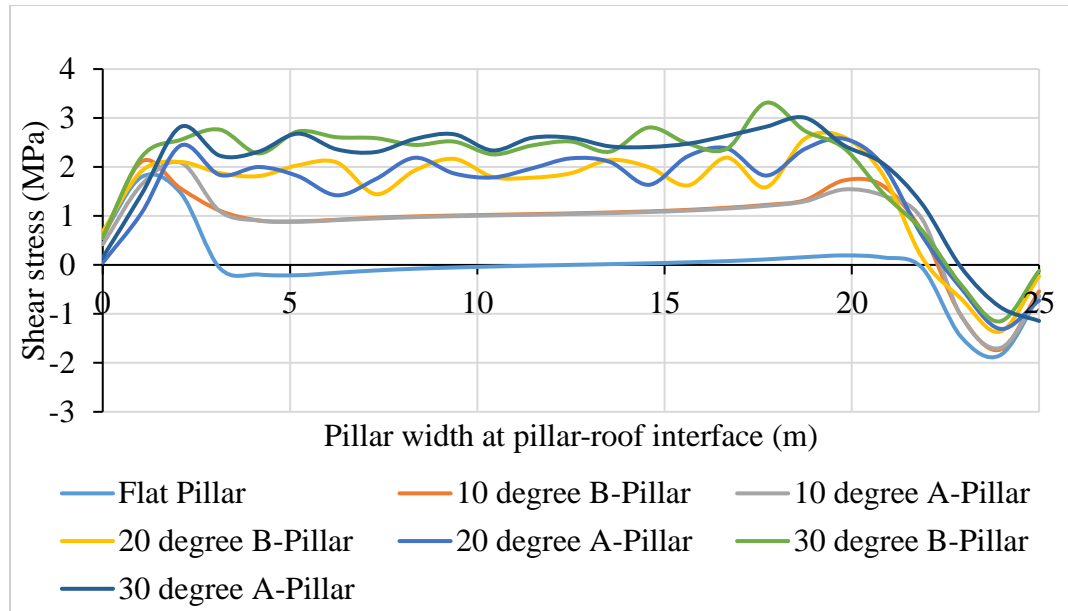


Figure 4.22: Variation of the shear stress along the pillar-roof interface with respect to the pillar inclination for Hoek & Brown models with coal UCS = 10 MPa.

In Figure 4.23 it is observed that at an inclination of 30° the uphill peak stresses in the pillar-roof interface are higher in pillars with perpendicular ribs (B-Pillar) than vertical ribs (A-Pillar). Throughout the width of the pillar the shear stresses remain the same for both pillar geometries.

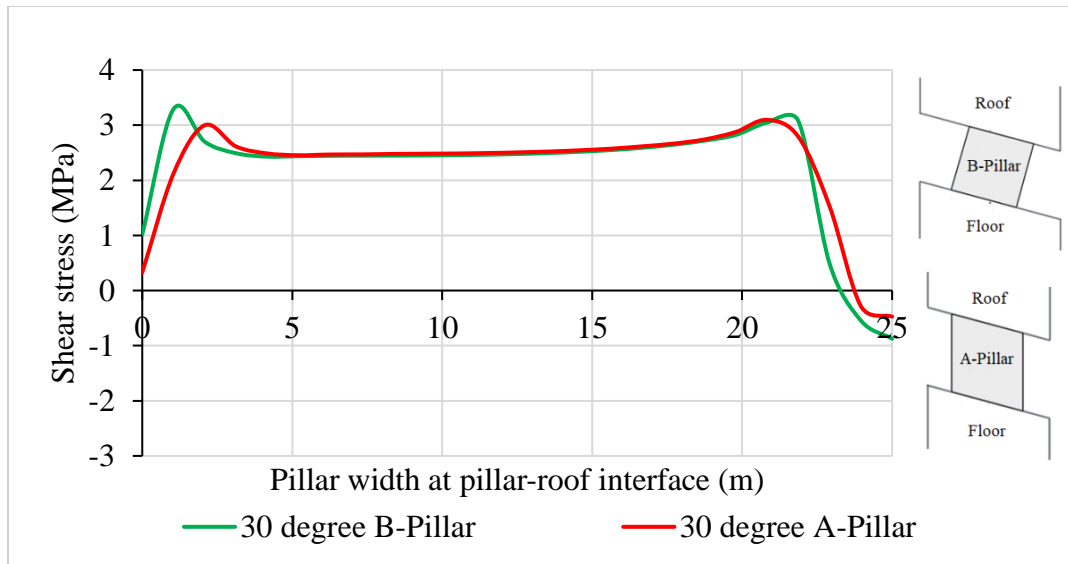


Figure 4.23: Variation of the shear stress along the pillar-roof interface with respect a 30° pillar inclination Hoek & Brown models with coal UCS = 20 MPa for A-Pillar and B-Pillar.

4.2.3 Comparison between the elastic and Hoek & Brown models

Figure 4.24 compares the shear stress between the elastic and Hoek & Brown models for a flat pillar and 20° inclined A-Pillar. At the pillar ribs higher peak shear stresses are observed in the elastic models compared to the Hoek & Brown models. This is due to the rib material that has yielded, and as a result, the peak stresses are translated more inward for the Hoek & Brown models.

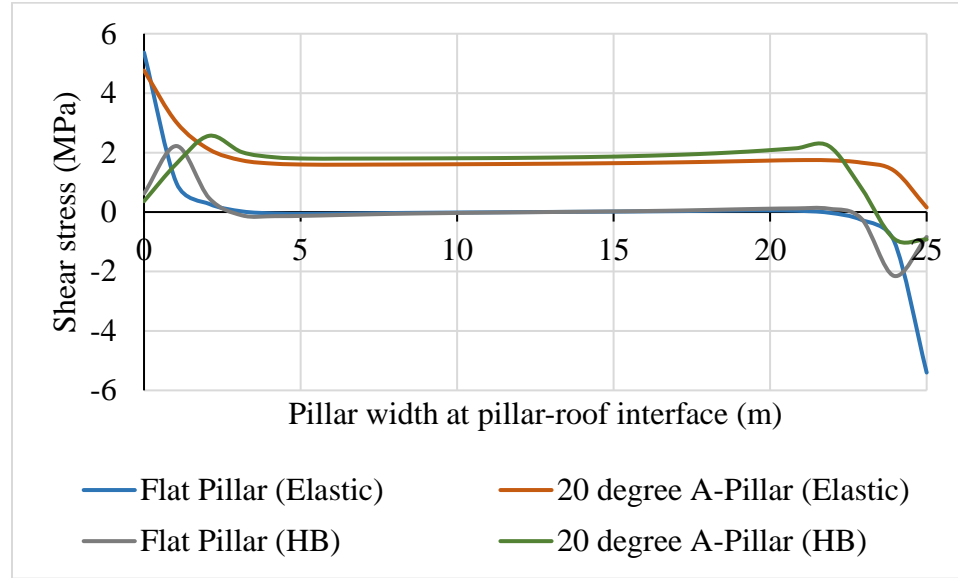


Figure 4.24: Comparison of the shear stress between the elastic and Hoek & Brown models for a flat pillar and 20° inclined A-Pillar.

4.3 Summary of numerical results

This section summarizes all the data and graphs presented in Section 4.1 and 4.2. The summary tables (Table 4.1, Table 4.2,

Table 4.3, Table 4.4) compare the peak stress, mid pillar stress and the location of the peak stress from the rib for all the models. The peak stress is the maximum stress experienced within the pillar and the mid pillar stress is the stress taken at the middle of the pillar or 12.5m from the rib. Table 4.1 and Table 4.2 summarize the major principal stress under elastic and Hoek & Brown conditions, while

Table 4.3 and Table 4.4 summarize the shear stress under elastic and Hoek & Brown conditions. In the case where lower coal UCS values were used at higher seam inclinations it seems that the strain softening model does not smoothly converge to a solution. Therefore, an average value was taken around the indicated location (mid pillar or peak stress) and is denoted by an “*” next to the value.

Table 4.1: Summary of the major principal stress results under elastic conditions.

Model	Peak Stress (MPa)	Mid pillar stress (MPa)	Location of the peak stress from the pillar rib (m)
Flat Pillar	10.63	7.97	0.758
10° A-Pillar	10.48	7.96	0.505
10° B-Pillar	10.49	7.97	0.758
20° A-Pillar	10.32	7.89	0.505
20° B-Pillar	10.17	7.92	0.758
30° A-Pillar	10.1	7.67	0.505
30° B-Pillar	9.23	7.72	1.01

Figure 4.25 compares the peak and the mid pillar major principal stress for models under elastic conditions. There is a slight decrease in the peak major principal stress when the seam inclination increases. The mid pillar principal stress is constant for all inclinations.

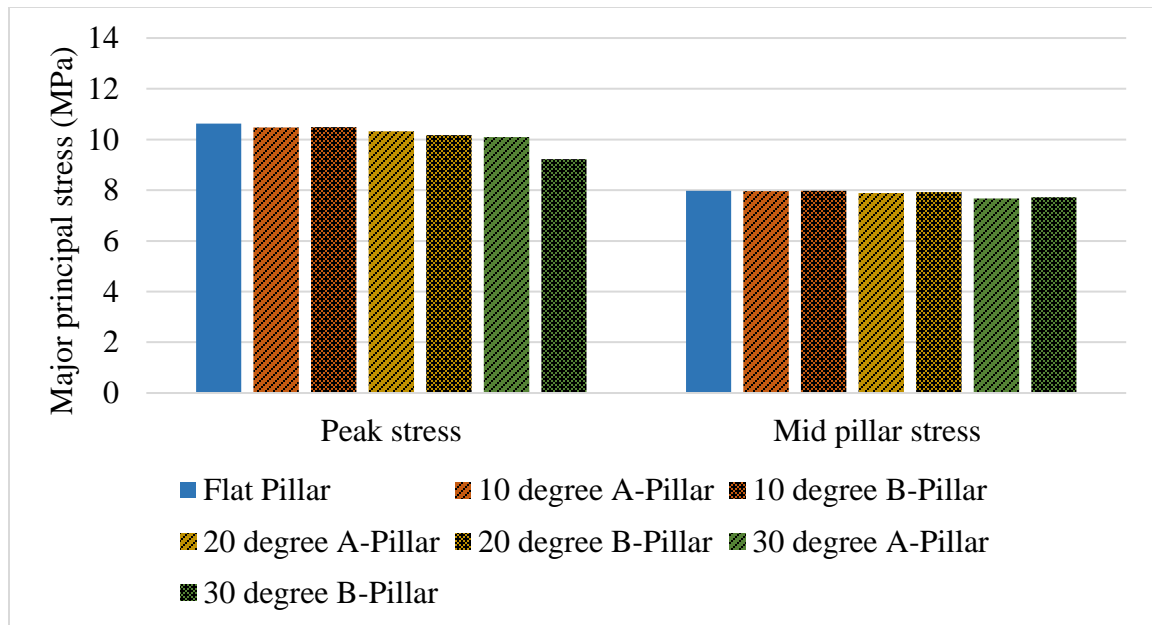


Figure 4.25: Major principal stress under elastic conditions.

Table 4.2 summarizes the major principal stress results under Hoek & Brown conditions.

Table 4.2: Summary of the major principal stress results under Hoek & Brown conditions.

Model	Peak Stress (MPa)	Mid pillar stress (MPa)	Location of the peak stress from the pillar rib
Coal UCS = 10 MPa			
Flat Pillar	11.694	8.76	3.03
10° A-Pillar	11.35	8.85	3.53
10° B-Pillar	11.37	8.879	3.28
20° A-Pillar	10.87	8.9*	4.042
20° B-Pillar	11.097	9*	3.788
30° A-Pillar	10.14	9.1*	4.032
30° B-Pillar	10.746	9*	3.788
Coal UCS = 15 MPa			
Flat Pillar	12.06	8.54	2.02
10° A-Pillar	12.108	8.54	2.52
10° B-Pillar	11.76	8.56	2.27
20° A-Pillar	10.956	8.6	2.782
20° B-Pillar	11.14	8.56	2.273
30° A-Pillar	10.18	8.7*	3.7
30° B-Pillar	10.695	8.58*	2.778
Coal UCS = 20 MPa			
Flat Pillar	13.28	8.39	1.768
10° A-Pillar	11.54	8.4	1.767
10° B-Pillar	12.6	8.41	1.768
20° A-Pillar	11.62	8.47	2.019
20° B-Pillar	11.118	8.4	1.768
30° A-Pillar	10.6	8.3	2.78
30° B-Pillar	10.7	8.23	2.02

Figure 4.26 compares the peak major principal stress under Hoek & Brown conditions for different coal UCS values. Through all the coal UCS models there is a common trend that the peak major principal stress decreases slightly as the seam inclination increases.

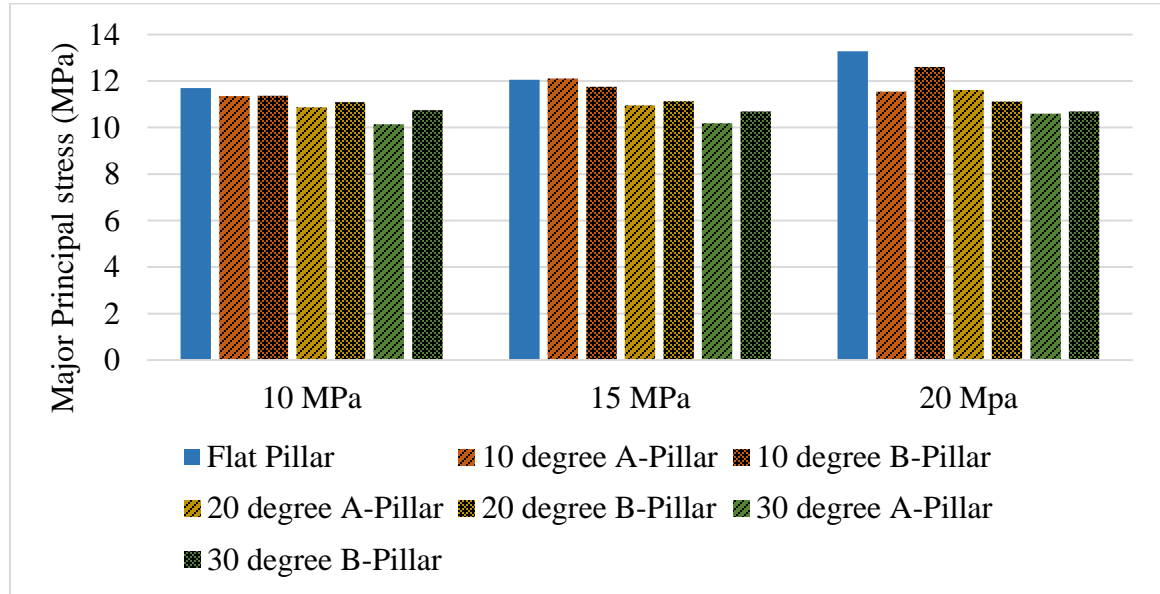


Figure 4.26: Peak major principal stress results under Hoek & Brown conditions.

Figure 4.27 compares the mid pillar major principal stress, under Hoek & Brown conditions, for different coal UCS values. The major principal stress for all the models is constant.

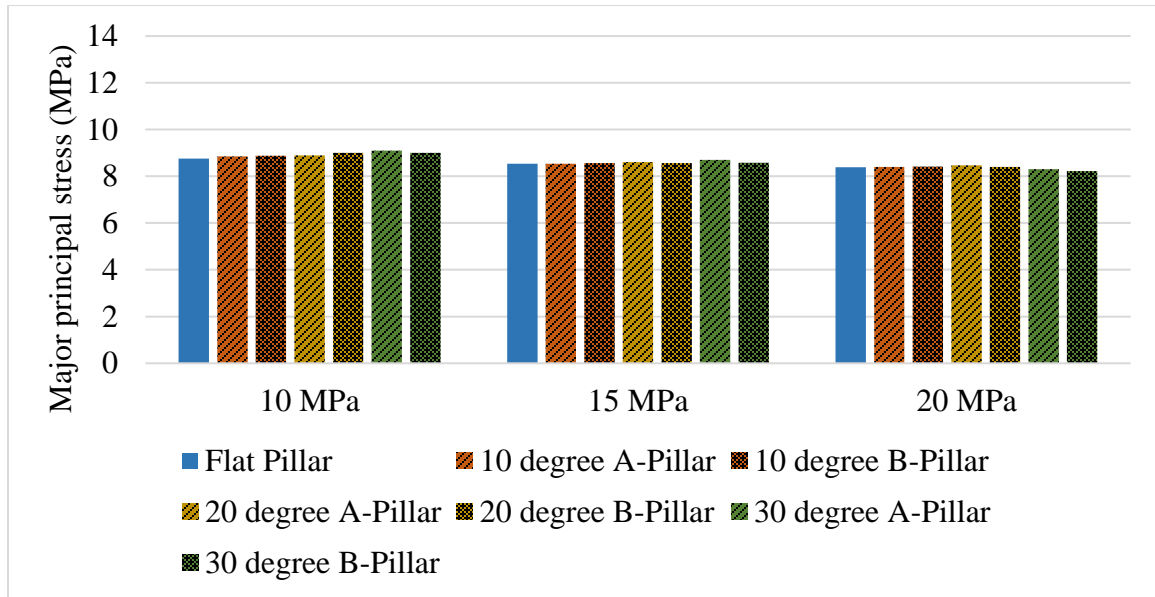


Figure 4.27: Mid pillar major principal stress results under Hoek & Brown conditions.

Table 4.3 summarizes the shear stress results under elastic conditions.

Table 4.3: Summary of the shear stress results under elastic conditions.

Model	Peak stress (MPa)	Mid pillar stress (MPa)	Location of the peak stress from the pillar rib (m)
Flat Pillar	5.36	0	0
10° A-Pillar	4.784	0.9	0
10° B-Pillar	5.6	0.9	0
20° A-Pillar	4.76	1.6	0
20° B-Pillar	7	1.6	0
30° A-Pillar	5.05	2.2	0
30° B-Pillar	6.2	2.2	0

Figure 4.28 shows the results of the peak and mid pillar shear stress under elastic conditions. When looking at the peak shear stress, there is a general trend where the B-

Pillar (perpendicular ribs) experiences higher shear stresses than the A-Pillar (vertical ribs). The shear stress in the middle of the pillar increases as the seam inclination increases.

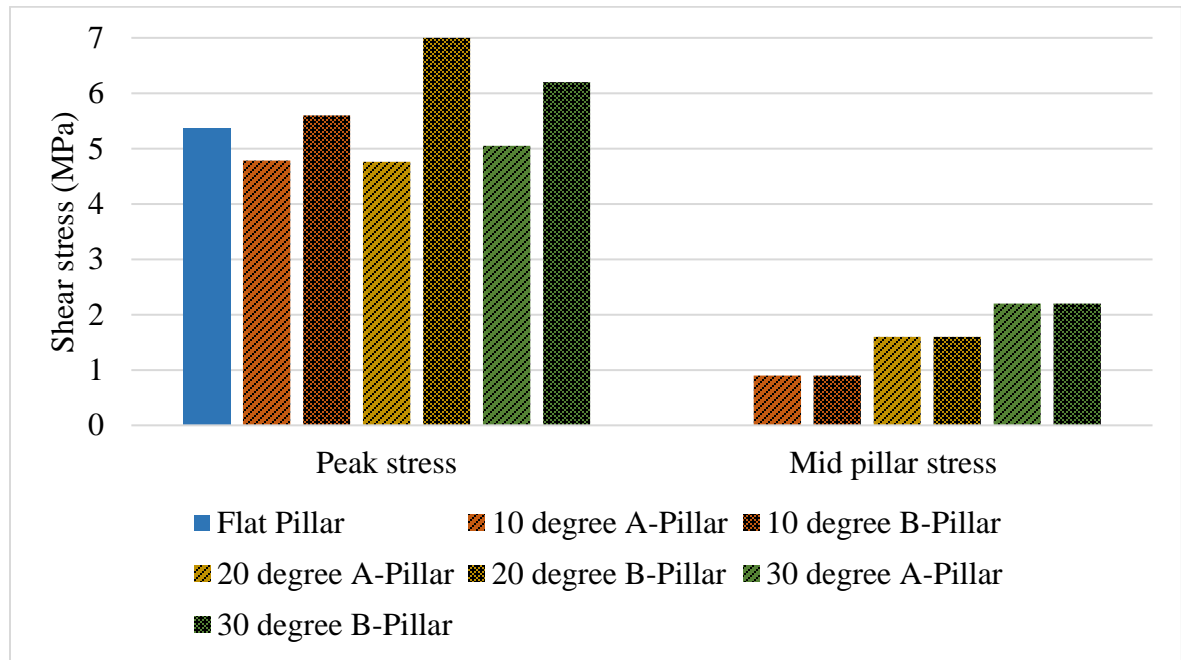


Figure 4.28: The peak and mid pillar shear stress results under elastic conditions.

Table 4.4 summarizes the shear stress results under Hoek & Brown conditions for different coal UCS values.

Table 4.4: Summary of the shear stress results under Hoek & Brown conditions.

Model	Peak stress (MPa)	Mid pillar stress (MPa)	Location of the peak stress from the pillar rib (m)
Coal UCS = 10 MPa			
Flat Pillar	1.798	0	1.042
10° A-Pillar	2.08	1.039	2.083
10° B-Pillar	2.11	1.05	1.042
20° A-Pillar	2.44	2.17*	2.083
20° B-Pillar	2.1	1.87*	2.083
30° A-Pillar	2.82	2.5*	2.083

30° B-Pillar	2.6	2.5*	2
Coal UCS = 15 MPa			
Flat Pillar	2.35	0	1.042
10° A-Pillar	2.16	0.97	1.042
10° B-Pillar	2.2	0.98	1.042
20° A-Pillar	2.84	1.89	2.083
20° B-Pillar	2.65	1.87	1.042
30° A-Pillar	2.59	2.5*	2.083
30° B-Pillar	2.8	2.5*	2.083
Coal UCS = 20 MPa			
Flat Pillar	2.22	0	1.042
10° A-Pillar	2.471	0.96	2.083
10° B-Pillar	2.82	0.96	1.042
20° A-Pillar	2.56	1.82	2.083
20° B-Pillar	2.86	1.8	1.042
30° A-Pillar	2.99	2.5	2.083
30° B-Pillar	3.3	2.5	1.042

Figure 4.29 shows the peak shear stress under Hoek & Brown conditions. A general trend through all the models is that as the seam inclination increases the peak shear stress increases. The 20 MPa UCS coal models shows a similar trend as the elastic models, where the B-Pillar (perpendicular ribs) experiences higher peak shear stresses than the A-Pillar (vertical ribs). This probably indicates that the coal material in these models has not failed due to applied loads. The 15 MPa and 10 MPa UCS coal models show a different behavior which can be attributed to coal material failure due to the applied loads.

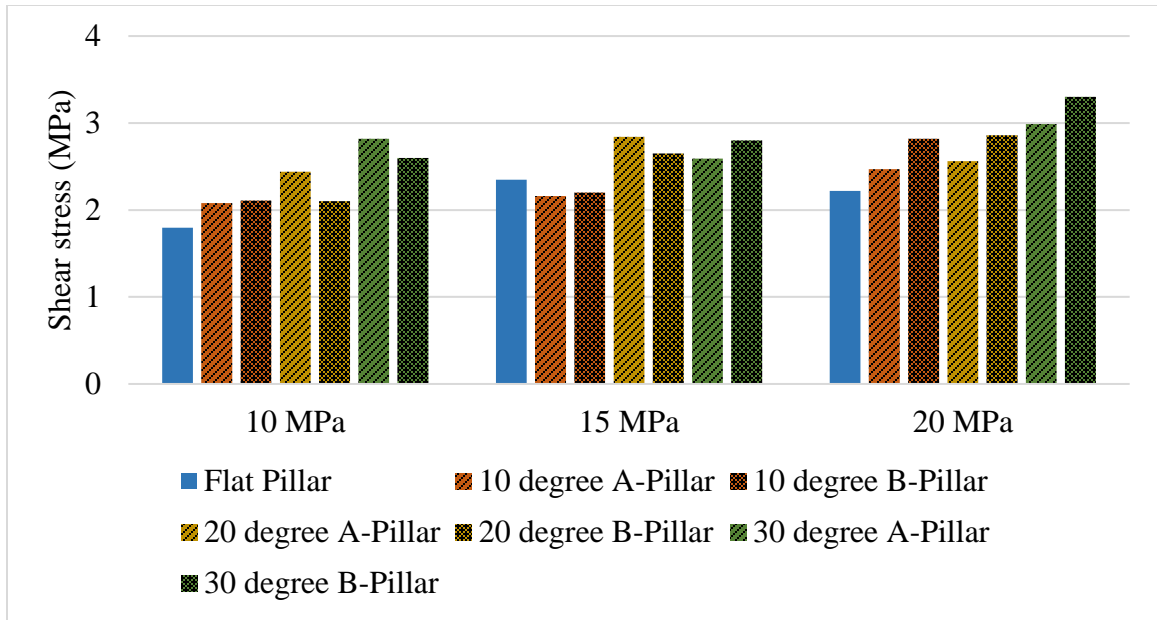


Figure 4.29: Peak shear stress results under Hoek & Brown conditions.

Figure 4.30 shows the mid pillar shear stress results under Hoek & Brown conditions for different coal UCS values. The general trend through all the models is that as the seam inclination increases the mid pillar shear stress increases.

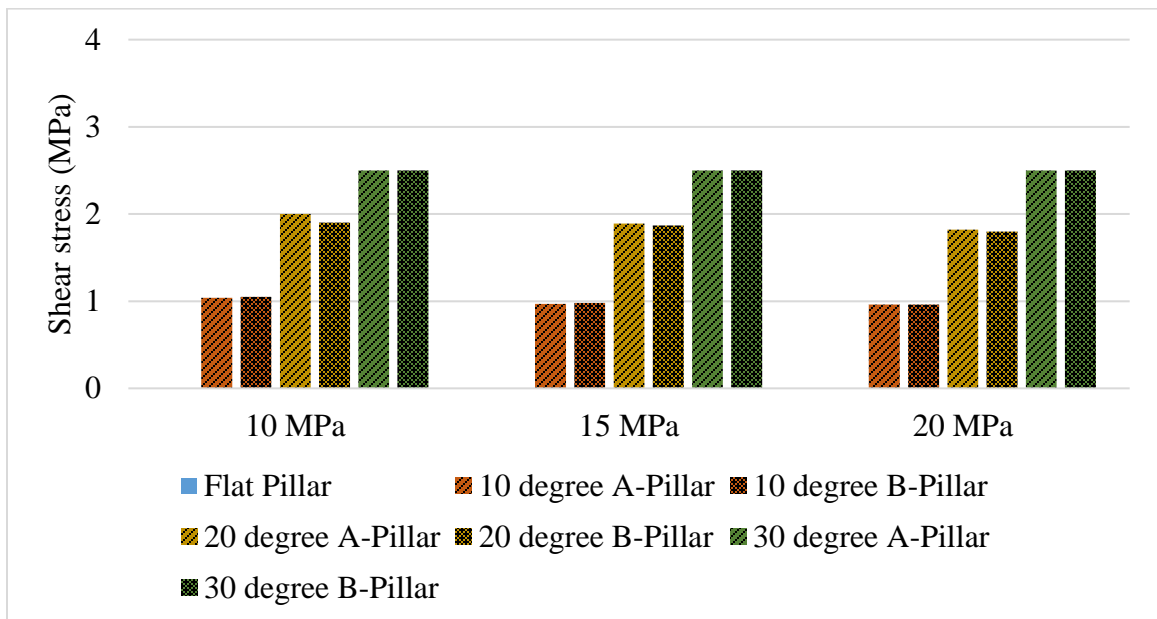


Figure 4.30: Mid pillar shear stress result under Hoek & Brown conditions.

CHAPTER 5. CONCLUSIONS AND RECOMMENDATIONS

5.1 Conclusions

Over the years numerous studies have been completed on square and rectangular pillars in horizontal seams, however very few studies are available with respect to pillars in inclined seams. Inclined pillars are subject not only to high normal stresses, but they are also subject to higher shear stresses that depend on the inclination of the seam, the ratio of the horizontal to vertical in-situ stress as well as the physical and mechanical properties of the material. The present work presented hypothetical elastic and Hoek & Brown numerical models, to investigate the major principal stress and shear stress at different seam inclinations.

The results from the elastic two-dimensional plane strain models for inclined pillars indicate the following:

- Major principal stress
 - The major principal stress developed in the pillar decreases slightly as the seam inclination increases.
 - The major principal stresses in the core of the pillar are the same for the A- and B-Pillar geometries.
 - The B-Pillar (perpendicular ribs) experiences lower principal stress at the pillar ribs compared to the A-Pillar (vertical ribs).
- Shear stress
 - The shear stress peak on the uphill side of the inclined pillars.
 - The shear stress increases as the seam inclination increases.
 - The shear stress is the same for the A- and B-Pillar geometry in the mid pillar. The B-Pillar (perpendicular ribs) experiences higher shear stress at the pillar ribs compared to the A-Pillar (vertical ribs).

The results from the Hoek & Brown two-dimensional plane strain models for inclined pillars indicate the following:

- Major principal stress
 - The location of the peak value of the major principal stress is translated more towards the core of the pillar compared to the results for elastic models.
 - The major principal stress at the ribs are higher for the elastic models than the Hoek & Brown models.
 - When the coal UCS decreases the major principal stress are translated more towards the core of the pillar.
 - Also, when the coal UCS decreases the yielding zones at the pillar ribs increases.

- Shear stress
 - The shear stress developed in the pillar roof interface for the Hoek & Brown models does not peak at the uphill pillar rib, compared to the elastic models.
 - The shear stress increases as the seam inclination increases.
 - The shear stress is the same for the A- and B-Pillar geometry, at the pillar roof interface.

5.2 Recommendations

The recommendations for future work include:

- The development of 3D models for flat and inclined geometries.
- The investigation of a greater range of UCS values so as to validate the different behavior between elastic and yielding models.
- The investigation of interface elements with different properties. This includes conditions when mining into the roof and the floor and not on the contact plane.
- The investigation of various vertical to horizontal stress ratios.
- The investigation of models that consider different material zones within a pillar may add value to this analysis.
- A comparison of the results with actual data collected by operators.

REFERENCES

- Aadnøy, B. S., & Looyeh, R. (2019). Insitu stress. In petroleum rock mechanics, p.105–144. Elsevier. <https://doi.org/10.1016/B978-0-12-815903-3.00008-X>.
- Bertuzzi, R. (2019). Estimating rockmass properties. PSM, Unit G, 3, p.56. Delhi Rd North Ryde New South Wales Australia.
- Bieniawski, Z. T. (1968). The effect of specimen size on compressive strength of coal. International Journal of Rock Mechanics and Mining Sciences & Geomechanics Abstracts, 5(4), p.325–335. [https://doi.org/10.1016/0148-9062\(68\)90004-1](https://doi.org/10.1016/0148-9062(68)90004-1).
- Bieniawski, Z. T. (1983). New design approach for room-and pillar coal mines in the USA (pp. E27–E36). Proceedings, 5th Congress International Society Rock Mechanics, Melbourne, Australia.
- Bieniawski, Z. T. (1984). Rock mechanics design in mining and tunneling. Balkema, Rotterdam.
- Brady, B. H. G., & Brown, E. T. (2006). Rock Mechanics for underground mining (3rd ed.). Springer Dordrecht, <https://doi.org/10.1007/978-1-4020-2116-9>.
- Cardenas Triana, C., Castillo, J., & Agioutantis, Z. (2021). Investigation of Coal Burst Potential Using a Finite Element Method Approach. Proceedings, 40th International Conference on Ground Control in Mining.
- Coates, D. (1981). Caving, subsidence, and ground control. Rock Mechanics Principles, CANMET, Department of Energy, Mines and Resources, Canada, p.1–5.
- Das, A. J., Mandal, P. K., Paul, P. S., & Sinha, R. K. (2019). Generalized Analytical Models for the Strength of the Inclined as well as the Flat Coal Pillars using Rock Mass Failure Criterion. Rock Mechanics and Rock Engineering, 52(10), p.3921–3946. <https://doi.org/10.1007/s00603-019-01788-7>.
- Elmo, D., & Stead, D. (2010). An Integrated Numerical Modelling–Discrete Fracture Network Approach Applied to the Characterization of Rockmass Strength of Naturally Fractured Pillars. Rock Mechanics and Rock Engineering, 43(1), p.3–19. <https://doi.org/10.1007/s00603-009-0027-3>.
- Esterhuizen, G. S. (2006). An evaluation of the strength of slender pillars. Transactions of Society for Mining, Metallurgy, and Exploration, Inc, 320, 69–76.
- Esterhuizen, G. S., Dolinar, D. R., & Ellenberger, J. L. (2008). Pillar strength and design methodology for stone mines. Proceedings, 27th International Conference on Ground Control in Mining, p.241–253.
- Fahrman, B. P. (2016). Numerical Modeling of Room-and-Pillar Coal Mine Ground Response. PhD Dissertation. Virginia Polytechnic Institute and State University.

- Foroughi, M. H. (1996). Some aspects of coal pillar stability in inclined coal seams. PhD Dissertation. University of New South Wales.
- Gaddy, F. L. (1956). A study of the ultimate strength of coal as related to the absolute size of the cubical specimens tested. PhD Dissertation. Virginia Polytechnic Institute and State University.
- Garza-Cruz, T., Pierce, M., & Board, M. (2019). Effect of shear stresses on pillar stability: A back analysis of the troy mine experience to predict pillar performance at Montanore Mine. *Rock Mechanics and Rock Engineering*, 52(12), p.4979–4996. <https://doi.org/10.1007/s00603-019-02011-3>.
- Greenwald, H., Howarth, H., & Hartmann, I. (1941). Experiments on strength of small pillars of coal in the Pittsburgh bed. US Bureau of Mines.
- Hedley, D. G. F., & Grant, F. (1972). Stope-and-pillar design for Elliot Lake Uranium Mines. *Bull. Can. Inst. Min. Metal.*, 65(723), p.37–44.
- Hedley, D. G. F., Roxburgh, J. W., & Muppalaneni, S. N. (1984). A case history of rock bursts at Elliot Lake. *Proceedings, Second International Conference on Stability in Underground Mining*, p.210–234.
- Herget, G. (1988). *Stresses in Rocks*. Rotterdam, Balkema, 179 p.
- Hoek, E., Carranza-Torres, C. and Corkum, B., 2002. Hoek-Brown failure criterion-2002 edition. *Proceedings of NARMS-Tac*, 1(1), pp. 267-273.
- Hoek, E., & Brown, E. T. (1980). *Underground excavation in Rock*. London Institution of Mining and Metallurgy, London, 527 p.
- Jeremic, M. L. (1985). *Strata Mechanics in Coal Mining*. Balkema, Rotterdam, Boston, The Netherlands.
- Jessu, K., Spearing, A., & Sharifzadeh, M. (2018). Laboratory and Numerical Investigation on Strength Performance of Inclined Pillars. *Energies*, 11(11), p.3229. <https://doi.org/10.3390/en11113229>.
- Jessu, K. V., & Spearing, A. J. S. (2019). Performance of inclined pillars with a major discontinuity. *International Journal of Mining Science and Technology*, 29(3), p.437–443. <https://doi.org/10.1016/j.ijmst.2018.09.006>.
- Jing, L., & Hudson, J. A. (2002). Numerical methods in rock mechanics. *International Journal of Rock Mechanics and Mining Sciences*, 39(4), p.409–427. [https://doi.org/10.1016/S1365-1609\(02\)00065-5](https://doi.org/10.1016/S1365-1609(02)00065-5).
- Kaiser, P. K., & Tang, C. A. (1998). Numerical Simulation of Damage Accumulation and Seismic Energy Release During Brittle Rock Failure—Part II: Rib Pillar Collapse. *International Journal of Rock Mechanics and Mining Sciences*, 35(2), p.123–134. [https://doi.org/10.1016/S0148-9062\(97\)00010-7](https://doi.org/10.1016/S0148-9062(97)00010-7)

- Kaklis, K., Agioutantis, Z., and G. Moitse. (2021). Pillar Stability Analysis for Partial Pillar Extraction. A Case Study at an Underground Coal Mine in Southern Africa. Proceedings, 55th U.S. Rock Mechanics/Geomechanics Symposium.
- Logie, C., & Matheson, G. (1982). A critical review of the current state-of-the-art design of mine pillars. Proceedings, 1st International Conference of Stability of Underground Mining, pp. 359–382.
- Lorig, L. J., & Cabrera, A. (2013). Pillar strength estimates for foliated and inclined pillars in schistose material. 3rd International FLAC/DEM Symposium, Hangzhou, China, p.22–24.
- Lunder, P. J., & Pakalnis, R. (1997). Determining the strength of hard rock mine pillars. Bull. Can. Inst. Min. Metall., 90, p.51–55.
- Luo, B., Ye, Y., Hu, N., & Wang, W. (2020). Investigation of Dip Effect on Uniaxial Compressive Strength of Inclined Rock Sample by Experimental and Theoretical Models. Rock Mechanics and Rock Engineering, 53(12), p.5659–5675.
<https://doi.org/10.1007/s00603-020-02234-9>.
- Maritz, J. A. (2015). Pillar Strength Adjustments in the Presence of Shear Stresses. Proceedings, 13th ISRM International Congress of Rock Mechanics.
- Mark, C. (2006). The evolution of intelligent coal pillar design. Proceedings, 25th International Conference on Ground Control in Mining, Morgantown, WV, pp. 325–334.
- Maritz, J. A. (2015). The effect of shear stresses on pillar strength. Master's thesis, University of Pretoria.
- Maybee, W. G. (2000). Pillar design in hard brittle rocks. School of Graduate Studies, Laurentian University.
- Mgumbwa, J. J., Suorineni, F. T., & Kaiser, P. K. (2010). Failure Mechanisms of Pillars Under Shear Loading. USDR, Tanzania, p.1–8.
- Obert, L., & Duvall, W. I. (1967). Rock mechanics and the design of structures in rock (Vol. 650). John Wiley & Sons Inc, New York.
- Pariseau, W. G. (1982). Shear stability of mine pillars in dipping seams. Proceedings, 23rd U.S Symposium on Rock Mechanics (USRMS).
- Peng, S. S. (1986). Coal Mine Ground Control. 2nd Edition. John Wiley & Sons.
- Poklopová, T., Pavelcová, V., & Šejnoha, M. (2021). Comparing the Hoek-Brown and Mohr-Coulomb failure criteria in fem analysis. Acta Polytechnica CTU Proceedings, 30, p.69–75. <https://doi.org/10.14311/APP.2021.30.0069>.

Rocscience Inc. (2022). Rocscience. Retrieved from RS2:
<https://www.rocscience.com/software/rs2>.

Saeidi, A., Cloutier, C., Kamalibandpey, A., & Shahbazi, A. (2022). Evaluation of the Effect of Geomechanical Parameters and In Situ Stress on Tunnel Response Using Equivalent Mohr-Coulomb and Generalized Hoek-Brown Criteria. *Geosciences*, 12(7), p.262. <https://doi.org/10.3390/geosciences12070262>.

Saiang, D., Gywnn, X. and Marshall, N., 2014. Hoek-Brown vs. Mohr-Coulomb: Results from a three-dimensional open-pit/underground interaction model. In *Bergmekanikdagen 2014*, Stockholm.

Salamon, M., & Munro, A. (1967). A study of the strength of coal pillars. *Journal of the Southern African Institute of Mining and Metallurgy*, 68(2), p.55–67.

Salamon, M., & Wagner, H. (1985). Practical experiences in the design of coal pillars. *Proceedings, 21st International Conference of Safety in Mines Research Institutes*, pp. 3–9.

Sheorey, P. (1992). Pillar strength considering in-situ stress. *Workshop on Coal Pillar Workshop on Coal Pillar Mechanics and Design*, Santa Fe, Ed. A.T. USBM IC 9315, pp. 122–127.

Sheorey, P. (1997). *Empirical Rock Failure Criteria*. Balkema. Rotterdam.

Sheorey, P. R. (1993). Design of Coal Pillar Arrays and Chain Pillars. In *Analysis and Design Methods* (p. 631–670). Elsevier. <https://doi.org/10.1016/B978-0-08-040615-2.50030-7>.

Sheorey, P. R., Das, M. N., Barat, D., Prasad, R. K., & Singh, B. (1987). Coal pillar strength estimation from failed and stable cases. *International Journal of Rock Mechanics and Mining Sciences & Geomechanics Abstracts*, 24(6), p.347–355.
[https://doi.org/10.1016/0148-9062\(87\)92256-X](https://doi.org/10.1016/0148-9062(87)92256-X).

Sheorey, P. R., Das, M. N., Bordia, S. K., & Singh, B. (1986). Pillar strength approaches based on a new failure criterion for coal seams. *International Journal of Mining and Geological Engineering*, 4(4), p.273–290. <https://doi.org/10.1007/BF01552957>.

Suorineni, F. T. (2013). Pillar design in underground mining. *Proceedings, 23rd World Mining Congress*.

Suorineni, F. T., Kaiser, P. K., Mgumbwa, J. J., & Thibodeau, D. (2011). Mining of orebodies under shear loading Part 1 – case histories. *Mining Technology*, 120(3), p.137–147. <https://doi.org/10.1179/1743286311Y.0000000012>.

Tulu, I., Esterhuizen, G., Mohamed, K. & Klemetti, T. (2017). Verification of a calibrated longwall model with field measurements. *Proceedings, 51st US Rock Mechanics/Geomechanics Symposium*, paper 17-238.

Trumbachev, V. F., & Melnikov, E. A. (1964). Distribution of stresses in the intervening pillars at medium and steep dip. Proceedings, 4th Cong. Strata control and rock mech., pp. 316–322.

Tuncay, D., Tulu, I.B., Klemetti, T. (2021). Investigating different methods used for approximating pillar loads in longwall coal mines, International Journal of Mining Science and Technology, Volume 31, Issue 1, pp. 23-32.
<https://doi.org/10.1016/j.ijmst.2020.12.007>.

Van der Merwe, J.N. (2003). New pillar strength formula for South African coal. Journal of the Southern African Institute of Mining and Metallurgy, 109(5), pp. 281–292.

Van der Merwe, J.N., Madden, B. J., & Buddery, P. (2002). Rock engineering for underground coal mining (2nd ed.). South African Institute of Mining and Metallurgy.

Van der Merwe, J. N. (1999). New strength formula for coal pillars in South Africa. Proceedings, Second international workshop on coal pillar mechanics and design, pp. 99–114.

Wilson, A. H. (1972). An hypothesis concerning pillar stability. The Mining Engineer, 131(1), p.409–417.

Wilson, A. H. (1983). The stability of underground workings in the soft rocks of the Coal Measures. International Journal of Mining Engineering, 1(2), p.91–187.
<https://doi.org/10.1007/BF00880785>.

York, G., Canbulat, I., & Jack, B. (2000). Coal pillar design procedures. Safety in Mine Research Advisory Committee, pp. 1–216.

VITA

Education

Pursuing a Master of Science in Mining Engineering at the University of Kentucky, Lexington, Kentucky. December 2022. Thesis Title: Parametric numerical analysis of inclined coal pillars.

Bachelor of Engineering (Honors), Engineering and Technology Management at the University of Pretoria, South Africa. December 2020.

Bachelor of Engineering, Mining Engineering at the University of Pretoria, South Africa. December 2019.

Employment

Graduate Research Assistant, Department of Mining Engineering, University of Kentucky. June 2022-December 2022.

Graduate Teaching Assistant, Department of Mining Engineering, University of Kentucky. January 2021-May 2022.

Mining Engineer I, Sasol Limited, Secunda, South Africa. January 2020 – December 2020.

Mining Engineer Intern, Anglo American Platinum, Amandelbult, South Africa, summer of 2017 and 2018.

Professional Honors and Awards

Recipient of Syd S. and Felicia F. Peng Ground Control in Mining Scholarship – Society for Mining, Metallurgy and Exploration (SME). December 2020.